# Equivalent imperfections for the out-of-plane stability design of steel beams by second-order inelastic analysis

Chunyan Quan*, Fiona Walport, Leroy Gardner

*Department of Civil and Environmental Engineering, South Kensington Campus, Imperial College London, London SW7 2AZ, UK*

* Corresponding author. E-mail address: c.quan17@imperial.ac.uk

**ABSTRACT**

In current structural design specifications, such as EN 1993-1-1 for steel and EN 1993-1-4 for stainless steel, the stability of members is typically assessed through the use of buckling curves, which consider the influence of initial geometric imperfections and residual stresses. An alternative, more direct, approach is to perform either an elastic or inelastic second-order analysis of the member or structure with imperfections. For modelling convenience, so-called 'equivalent' imperfections are typically utilised, which consider the combined influence of both geometric imperfections and residual stresses. Equivalent imperfections for the design of columns and beams by second-order elastic analysis, also referred to as geometrically nonlinear analysis with imperfection (GNIA), are provided in the current design specifications. For columns, equivalent imperfections for design by second-order inelastic analysis, also referred to as geometrically and materially nonlinear analysis with imperfections (GMNIA), were recently developed, but for beams that are susceptible to lateral-torsional buckling (LTB), there are currently no appropriate provisions. The aim of this study is therefore to develop equivalent imperfections for use in out-of-plane stability design of steel and stainless steel members by GMNIA. The proposals are calibrated against the results of benchmark finite element (FE) simulations performed on a large number of steel and stainless steel members with geometric imperfections and residual stresses subjected to major axis bending. Two proposals for equivalent imperfection amplitudes are developed: (1) $e_{0,\mathrm{mod}}$, for use with eigenmode-affine

imperfections and (2) $e_{0,bow}$, for use with sinusoidal bow imperfections. The latter is applied solely in the lateral direction and as a summation of a half-sine wave and a full sine wave. Relative to the traditional Eurocode design calculations, employing the proposed LTB imperfections in GMNIA provides generally more accurate member resistance predictions, while remaining safe-sided relative to the benchmark FE results. The reliability of the design provisions is demonstrated through statistical analysis, where it is shown that partial safety factors of 1.0 for steel and 1.1 for stainless steel can be safely adopted.

**Keywords:** Advanced analysis; Equivalent imperfections; Finite element modelling; Inelastic analysis; Lateral-torsional buckling; Plastic design; Stainless steel; Steel

## 1. INTRODUCTION

Steel beams are often susceptible to out-of-plane instability effects, such as lateral-torsional buckling (LTB). The influence of LTB on the resistances of steel beams is traditionally accounted for in design standards [1, 2] through the use of buckling curves. There are currently two different sets of LTB curves given in Eurocode 3 [1], referred to as the general case (see Section 2.1.1) and the specific case (see Section 2.1.2). These curves implicitly consider the influence of geometric imperfections and residual stresses in the determination of the buckling reduction factor [3-7]. Alternatively, the LTB design of members can be undertaken more directly by performing a second-order, also referred to as geometrically nonlinear, or advanced, analysis with imperfections. In this design approach, member out-of-straightness is explicitly modelled and individual member buckling checks can be avoided; only cross-section strength checks against internal forces derived according to second order theory are required, resulting in a more direct design approach.

In structural steel members, both geometric and material (i.e. residual stresses) initial imperfections arise during the manufacturing and fabrication processes, and the influence of

both must be accounted for in design. The required imperfection amplitude for use in design by advanced analysis depends on (i) the analysis type, (ii) the cross-section failure criterion and (iii) the shape of the imperfection modelled. Geometric imperfections can either be included in an analysis through direct modelling of the deformed geometry or through the scaling of a suitable eigenmode. In the former case, the relative simplicity of defining the deformed geometry is retained without the encumbrance of an additional linear buckling analysis (LBA), while in the latter case, more accurate results are generally achieved (see Section 5.2 for further details).

With improvements in computational efficiency, second-order inelastic analysis, also referred to as geometrically and materially nonlinear analysis with imperfections (GMNIA), typically implemented using computationally efficient beam finite elements, is being increasingly employed in the design of steel and stainless steel structures [8-11]. While EN 1993-1-1 [1] and the upcoming prEN 1993-1-1 [12] include recommendations for equivalent imperfections, which consider the combined influence of geometric imperfections and residual stresses, for use in second-order elastic analysis, there are currently no provisions for second-order inelastic analysis.

Equivalent imperfections have been developed by Walport et al. [13] for use in design by second-order inelastic analysis of structural members for flexural buckling. This study follows a similar methodology and derives equivalent imperfections for use in design by second-order inelastic analysis of structural members for LTB. Two equivalent imperfection amplitudes are proposed: (1) $e_{0,\mathrm{mod}}$, for use with the first LTB eigenmode and (2) $e_{0,\mathrm{bow}}$, for use with directly defined sinusoidal bow imperfections.

## 2. EUROCODE PROVISIONS FOR LTB DESIGN

In this section, the Eurocode provisions [1, 2, 12, 14] for design of beams susceptible to LTB are outlined. Firstly, the traditional approach for the LTB assessment of steel and stainless steel beams (i.e. the approach involving the calculation of the LTB reduction factor $\chi_{LT}$) is described; next, the current and upcoming provisions for LTB design by second-order elastic analysis using equivalent imperfections are set out. Finally, the need for revised equivalent imperfections for use in design by second-order inelastic analysis is explained.

### *2.1 EN 1993-1-1 design rules for laterally-unrestrained beams*

The current version of EN 1993-1-1 [1] considers two cases for the LTB assessment of steel beams – (i) a general case and (ii) a specific case, for rolled sections or equivalent welded sections. In both cases, the member buckling resistance $M_{b,Rd}$ is given by Eq. (1):

$$M_{b,Rd} = \chi_{LT} \frac{M_{c,Rk}}{\gamma_{M1}} \tag{1}$$

where $\chi_{LT}$ is the buckling reduction factor, which considers the adverse effects of LTB on the ultimate cross-section resistance of a steel beam, $\gamma_{M1}$ is the partial safety factor for member buckling, and $M_{c,Rk}$ is the characteristic (unfactored) cross-section bending moment resistance equal to the product of the yield stress $f_y$ and the major axis section modulus $W_y$ (i.e. $M_{c,Rk} = W_y f_y$); $W_y$ is taken as the plastic section modulus $W_{pl,y}$ for Class 1 and 2 cross-sections, the elastic section modulus $W_{el,y}$ for Class 3 cross-sections and an effective section modulus $W_{eff,y}$ for Class 4 cross-sections.

#### *2.1.1 General case*

The general case is applicable to beams with any cross-section type. The corresponding buckling curves are the same as those employed for column design, but a different buckling curve selection table is used [19]. In this approach, the LTB reduction factor $\chi_{LT}$ is calculated as:

$$\chi_{\mathrm{LT}} = \frac{1}{\phi_{\mathrm{LT}} + \sqrt{\phi_{\mathrm{LT}}^2 - \bar{\lambda}_{\mathrm{LT}}^2}} \leq 1 \tag{2}$$

where

$$\phi_{\mathrm{LT}} = 0.5\left[1 + \alpha_{\mathrm{LT}}\left(\bar{\lambda}_{\mathrm{LT}} - 0.2\right) + \bar{\lambda}_{\mathrm{LT}}^2\right], \tag{3}$$

in which $\alpha_{\mathrm{LT}}$ is the imperfection factor determined on the basis of the cross-section depth-to-width ($h/b$) ratio and $\bar{\lambda}_{\mathrm{LT}}$ is the non-dimensional slenderness, given by:

$$\bar{\lambda}_{\mathrm{LT}} = \sqrt{M_{\mathrm{c,Rk}} / M_{\mathrm{cr}}}, \tag{4}$$

in which $M_{\mathrm{cr}}$ is the elastic critical buckling moment determined either through numerical methods using a linear buckling analysis (LBA) or using approximate equations, for example those given in technical report CEN TR 1993-1-103 [15]; the latter approach has been adopted in this study. The current version of EN 1993-1-4 [2] also adopts the buckling curves described above for the design of stainless steel beams, but with $\alpha_{\mathrm{LT}} = 0.76$ (for welded I-sections) and a threshold (plateau) slenderness value of 0.4 instead of 0.2.

*2.1.2 Specific case*

The specific case is applicable to steel beams with rolled I-sections or equivalent welded I-sections. The LTB reduction factor $\chi_{\mathrm{LT}}$ can be determined as follows:

$$\chi_{\mathrm{LT}} = \frac{1}{\phi_{\mathrm{LT}} + \sqrt{\phi_{\mathrm{LT}}^2 - \beta\bar{\lambda}_{\mathrm{LT}}^2}} \text{ but } \chi_{\mathrm{LT}} \leq \begin{cases} 1 \\ 1/\bar{\lambda}_{\mathrm{LT}}^2 \end{cases} \tag{5}$$

where

$$\phi_{\mathrm{LT}} = 0.5\left[1 + \alpha_{\mathrm{LT}}\left(\bar{\lambda}_{\mathrm{LT}} - \bar{\lambda}_{\mathrm{LT,0}}\right) + \beta\bar{\lambda}_{\mathrm{LT}}^2\right] \tag{6}$$

in which $\beta$ is a modification factor and $\bar{\lambda}_{\mathrm{LT,0}}$ is the threshold (plateau) slenderness value, for which the value of 0.4 is recommended [1]. For non-uniform bending cases, in addition to the consideration through $M_{\mathrm{cr}}$, the applied LTB reduction factor may also be modified to take account of the full influence of the bending moment distribution [1]. The formulation of the

specific case is based on extensive experimental results [16], statistical work [17] and numerical studies [18], and differs from the flexural buckling curves.

Both the general case and specific case are modified Ayrton-Perry type formulae, calibrated for LTB through modification of the imperfection factor $\alpha_{\mathrm{LT}}$ [7]. For both hot-rolled and welded I-sections, the values of $\alpha_{\mathrm{LT}}$ prescribed for use with Eqs. (5) and (6) are higher than those for Eqs. (2) and (3).

*2.2 prEN 1993-1-1 and prEN 1993-1-4: Doubly symmetric I- and H-sections*

Unlike the flexural buckling curves, the LTB curves outlined in Section 2.1 are not fully mechanically coherent [19]. To address this issue, Taras and Greiner [7, 19] proposed a new set of formulae for the LTB design of steel members, as given by Eqs. (7) and (8), that are due to be included in the upcoming prEN 1993-1-1 [12],

$$\chi_{\mathrm{LT}} = \frac{f_{\mathrm{M}}}{\phi_{\mathrm{LT}} + \sqrt{\phi_{\mathrm{LT}}^2 - f_{\mathrm{M}}\bar{\lambda}_{\mathrm{LT}}^2}} \leq 1 \tag{7}$$

with

$$\phi_{\mathrm{LT}} = 0.5\left[1 + f_{\mathrm{M}}\left(\left(\frac{\bar{\lambda}_{\mathrm{LT}}}{\bar{\lambda}_{\mathrm{z}}}\right)^2 \alpha_{\mathrm{LT}}\left(\bar{\lambda}_{\mathrm{z}} - 0.2\right) + \bar{\lambda}_{\mathrm{LT}}^2\right)\right] \tag{8}$$

where $f_{\mathrm{M}}$ is a factor that accounts for the influence of bending moment diagram and $\bar{\lambda}_{\mathrm{z}}$ is the normalised member slenderness for minor axis flexural buckling. The definition of the imperfection factor $\alpha_{\mathrm{LT}}$ was also amended, becoming a function of the major $W_{\mathrm{el,y}}$ and minor axis $W_{\mathrm{el,z}}$ elastic section moduli of the beam cross-section, as listed in Table 1.

The new provisions shift the transition point between buckling curves (i.e. $\alpha_{\mathrm{LT}}$ value) from $h/b = 2.0$ to 1.2 to reflect the $h/b$ ratio at which a change in residual stress magnitude is assumed [20], while the geometric factor $\sqrt{W_{\mathrm{el,y}}/W_{\mathrm{el,z}}}$ considers the influence of varying cross-section geometry and reduces the scatter of the capacity predictions [7, 19]. An upper limit is

also defined, taken as the imperfection factor for minor axis buckling $\alpha_z$, on the basis that the compression flange of a very deep section with (comparatively) low torsional rigidity should behave similarly to a column undergoing minor axis buckling [7].

Taking the same expressions (i.e. Eqs. (7) and (8)), Fortan and Rossi [21] determined suitable $\alpha_{LT}$ values for application in the LTB design of stainless steel members; the proposals, given by Table 1, are due to be included, together with the indicated upper bounds, in the upcoming Eurocode prEN 1993-1-4 [14].

### *2.3 Equivalent imperfections for use in design by second-order elastic analysis*

Equivalent imperfections implicitly account for the combined effects of geometric and material imperfections. They may be applied in an analysis in two ways: (1) through the scaling of the lowest eigenmode or (2) through the direct modelling of a bow imperfection, and with an amplitude either determined by back-calculation from the relevant buckling curve or taken from a set of prescribed tabulated values. The equivalent imperfections developed for use in second-order elastic analysis (i.e. GNIA) are described in the following section.

#### *2.3.1 Back-calculated equivalent imperfections*

##### *2.3.1.1 EN 1993-1-1 back-calculated equivalent imperfections*

For the design by second-order elastic analysis of a steel beam susceptible to LTB, EN 1993-1-1 [1] recommends an equivalent imperfection with a lateral bow shape and an amplitude $ke_0$, where $e_0$ is the equivalent imperfection for the weak axis flexural buckling design of the corresponding member in compression and $k$ = 0.5. The amplitude $e_0$ can be back-calculated from the flexural buckling curves given in EN 1993-1-1 [1], as given by:

$$e_0 = \alpha_z \left(\bar{\lambda}_z - 0.2\right)\frac{W_z}{A} \quad \text{for } \bar{\lambda}_z \geq 0.2 \tag{9}$$

In Eq. (9), $\alpha_z$ is the imperfection factor for minor axis flexural buckling, $W_z$ is the minor axis section modulus and $A$ is the cross-sectional area. This equation was derived on the basis of a linear M-N cross-section failure criterion, under axial load $N$ and second-order minor axis bending moment $M_z$, as described in [22]. The linear elastic and plastic cross-section M-N interaction curves for axial force and minor axis bending moment are given by Eqs. (10) and (11), respectively:

$$\frac{N}{N_{\mathrm{pl}}}+\frac{M_{\mathrm{z}}}{M_{\mathrm{el,z}}}=1 \tag{10}$$

$$\frac{N}{N_{\mathrm{pl}}}+\frac{M_{\mathrm{z}}}{M_{\mathrm{pl,z}}}=1 \tag{11}$$

where $N_{\mathrm{pl}}$ is the axial cross-section resistance, and $M_{\mathrm{el,z}}$ and $M_{\mathrm{pl,z}}$ are the elastic and plastic minor axis bending moment resistances. For LTB design by GNIA, the linear elastic and plastic cross-section interaction curves are given by Eqs. (12) and (13), respectively [12, 23]:

$$\frac{M_{\mathrm{y}}}{M_{\mathrm{el,y}}}+\frac{M_{\mathrm{z}}}{M_{\mathrm{el,z}}}+\frac{B}{B_{\mathrm{el}}}=1 \tag{12}$$

$$\frac{M_{\mathrm{y}}}{M_{\mathrm{pl,y}}}+\frac{M_{\mathrm{z}}}{M_{\mathrm{pl,z}}}+\frac{B}{B_{\mathrm{pl}}}=1 \tag{13}$$

where $M_{\mathrm{y}}$ and $M_{\mathrm{z}}$ are the major and minor axis bending moments, $B$ is the bimoment, $M_{\mathrm{el,y}}$ and $M_{\mathrm{pl,y}}$ are the elastic and plastic major axis bending moment resistances and $B_{\mathrm{el}}$ and $B_{\mathrm{pl}}$ are the elastic and plastic warping bimoment resistances [24], as given for I-sections by:

$$B_{\mathrm{el}}=t_{\mathrm{f}}b^2 f_{\mathrm{y}}\left(h-t_{\mathrm{f}}\right)/6 \tag{14}$$

$$B_{\mathrm{pl}}=t_{\mathrm{f}}b^2 f_{\mathrm{y}}\left(h-t_{\mathrm{f}}\right)/4 \tag{15}$$

where $h$, $b$ and $t_{\mathrm{f}}$ are the overall depth, flange width and flange thickness of the I-section.

For flexural buckling, use of the back-calculated equivalent imperfection amplitudes – $e_{0,\mathrm{el,b\text{-}c}}$ (with a linear elastic cross-section check – Eq. (10)) and $e_{0,\mathrm{pl,b\text{-}c}}$ (with a linear plastic cross-section check – Eq. (11)) – in design by second-order elastic analysis (GNIA) yields the same

flexural buckling resistances as those obtained from the flexural buckling curves provided in EN 1993-1-1 [1]. However, for LTB design by second-order elastic analysis, the equivalent imperfections – $ke_{0,\mathrm{el,b\text{-}c}}$ and $ke_{0,\mathrm{pl,b\text{-}c}}$ – do not directly correspond to the results obtained from the buckling curves (clauses 6.3.2.2 and 6.3.2.3 of EN 1993-1-1 [1]), and have been shown to be inaccurate for use in LTB design by GNIA, with the value of $k = 0.5$ deemed to be too small [25].

*2.3.1.2 Equivalent imperfections back-calculated from LTB curves in prEN 1993-1-1*

According to the analytical formulation [7, 19] behind the new LTB curves given in prEN 1993-1-1 [12], the amplitude of the equivalent imperfection for use in GNIA $e_{0,\mathrm{LT}}$ [26] can be back-calculated from:

$$e_{0,\mathrm{LT}} = \alpha_{\mathrm{LT}}\left(\bar{\lambda}_{\mathrm{z}} - 0.2\right)\frac{W_{\mathrm{z}}}{A} \quad \text{for } \bar{\lambda}_{\mathrm{z}} \geq 0.2 \tag{16}$$

where $\alpha_{\mathrm{LT}}$ is the imperfection factor for LTB, determined from Table 1. Eq. (16) was derived on the basis of linear cross-section failure criterion under uniform major axis bending moment $M_{\mathrm{y}}$, second-order minor axis bending moment $M_{\mathrm{z}}$ and warping bimoment $B$ [7], as given by Eqs. (12) and (13). Employment of the elastic $W_{\mathrm{el,z}}$ and plastic $W_{\mathrm{pl,z}}$ minor axis section moduli in Eq. (16) provides the equivalent imperfections $e_{0,\mathrm{LT,el,b\text{-}c}}$ and $e_{0,\mathrm{LT,pl,b\text{-}c}}$, for use in GNIA with linear elastic (Eq. (12)) and plastic (Eq. (13)) cross-section verifications, respectively. Since the derivation of the LTB curves in prEN 1993-1-1 [12] was performed on the basis of eigenmode-affine imperfections, these back-calculated equivalent imperfections should also be defined through the scaling of the eigenmode in GNIA.

Fig. 1 (a) and (b) present the normalised second-order internal moments at the critical cross-section and linear cross-section interaction curves for members subjected to uniform major axis bending, obtained from GNIA and GMNIA employing equivalent imperfections $e_{0,\mathrm{LT,el,b\text{-}c}}$ and $e_{0,\mathrm{LT,pl,b\text{-}c}}$, as well as the prEN 1993-1-1 member buckling resistances $M_{\mathrm{EC3}}$. Fig. 1 (a) presents

the results for a Class 3 cross-section, which utilises a linear elastic cross-section interaction curve, while Fig. 1 (b) presents the results for a Class 2 cross-section, which utilises a linear plastic cross-section interaction curve. In both cases, the second-order elastic moment path with back-calculated imperfections intersects the interaction curve exactly at the buckling resistance $M_{\mathrm{EC3}}$, though this is not always the case due to the post-critical response of slender beams described below. However, as in the case of flexural buckling [13], the back-calculated equivalent imperfections determined for use in LTB design by GNIA are not suitable for use in GMNIA. Depending on the design case, the GNIA-derived equivalent imperfections can result in both over-predictions and under-predictions of resistance. In Fig. 1 (a), due to the spread of plasticity through the cross-section after first yield and before the attainment of the peak load, the member resistance obtained from GMNIA with $e_{0,\mathrm{LT,el,b\text{-}c}}$ is higher than the result obtained from GNIA with $e_{0,\mathrm{LT,el,b\text{-}c}}$. In Fig. 1 (b), due to the effective double-counting of the influence of material nonlinearity, utilising the plastic equivalent imperfection $e_{0,\mathrm{LT,pl,b\text{-}c}}$ in GMNIA results in a lower member resistance than that obtained from GNIA.

Note that, for some slender members, the ultimate resistance can exceed the elastic buckling moment $M_{\mathrm{cr}}$. This is because after large torsional deformations, the cross-sectional minor axis bending capacity effectively becomes a lower bound to the LTB resistance [7]. This behaviour is captured in a second-order analysis. However, the derivation of the LTB curves presented in prEN 1993-1-1 [12] and thus the equivalent imperfections back-calculated from the LTB curves, as determined by Eq. (16), do not account for this “post-critical” load-carrying mechanism [19]. Therefore, member resistances obtained from GNIA or GMNIA using back-calculated equivalent imperfections can be substantially exceed the prEN 1993-1-1 buckling resistance $M_{\mathrm{EC3}}$ [27], but only after large torsional deformations. This is shown in Fig. 2, for a hot-rolled S420 steel HEA 100 member with $\bar{\lambda}_{\mathrm{LT}}$ = 1.0 subjected to uniform bending. It can be seen that the member resistances obtained from GNIA and GMNIA with a back-calculated

equivalent imperfection $e_{0,\mathrm{LT,pl,b\text{-}c}}$ for the linear plastic cross-section interaction curve are higher than the Eurocode resistance $M_{\mathrm{EC3}}$ by 14% and 12%, respectively.

*2.3.2 Tabulated equivalent imperfections*

*2.3.2.1 EN 1993-1-1 tabulated equivalent imperfections*

According to EN 1993-1-1 [1], when using lateral bow equivalent imperfections of amplitude $ke_0$ in design by second-order elastic analysis, $e_0$ may, as a simpler alternative to performing the back-calculation described above, be taken from the tabulated values listed in Table 5.1 of EN 1993-1-1 [1] for the weak axis flexural buckling design of the corresponding member in compression; in prEN 1993-1-1 [12], revised tabulated equivalent imperfections for LTB design by second-order elastic analysis are provided [28], as described below.

*2.3.2.2 prEN 1993-1-1 tabulated equivalent imperfections*

According to prEN 1993-1-1 [12], equivalent imperfection amplitudes $e_{0,\mathrm{LT}}$ for use in LTB design by GNIA can be determined from Eq. (17):

$$e_{0,\mathrm{LT}} = \frac{\beta_{\mathrm{LT}} L}{\varepsilon} \tag{17}$$

where $\beta_{\mathrm{LT}}$ is the reference relative bow imperfection for LTB, values of which are provided in tabular form [12, 28], as summarised in Table 2, $L$ is the member length and $\varepsilon$ is the material parameter given by:

$$\varepsilon = \sqrt{\frac{235}{f_{\mathrm{y}}}} \tag{18}$$

The imperfection amplitude may be applied in the form of a lateral bow. Note that, unlike the corresponding equivalent imperfections for flexural buckling, given by Eq. (19), that are dependent on not only the reference relative bow imperfection for flexural buckling $\beta$, but also the imperfection factor $\alpha$ [29], Eq. (17) is not dependent on the LTB imperfection factor $\alpha_{\mathrm{LT}}$.

The factor $\beta_{\mathrm{LT}}$ in Eq. (17) does however depend on the adopted cross-section failure criterion (linear elastic or linear plastic) and the geometrical depth-to-width ratio $h/b$ of the cross-section.

$$e_0 = \frac{\alpha\beta L}{\varepsilon} \tag{19}$$

The use of Eq. (17) for LTB design by second-order elastic analysis has been shown in previous research [27, 30] to provide somewhat conservative resistance predictions. This is highlighted in Fig. 3, which shows the normalised load paths and capacity predictions of a hot-rolled S420 steel IPE 140 member with $\bar{\lambda}_{\mathrm{LT}}$ = 0.8 subjected to uniform bending. Employing the tabulated imperfection for use with the plastic interaction curve determined from Eq. (17) $e_{0,\mathrm{LT,pl,tab}}$ in both GNIA and GMNIA results in conservative resistance predictions, up to 17% lower than the prEN 1993-1-1 member buckling resistance $M_{\mathrm{EC3}}$. These tabulated imperfection amplitudes have been derived on the basis of second-order elastic analysis and, as for the back-calculated imperfection amplitudes and as in the case of flexural buckling [13], are generally unsuitable for use in design by second-order inelastic analysis (GMNIA).

## 3. GENERATION OF BENCHMARK FINITE ELEMENT DATA

In this section, benchmark finite element (FE) data, against which the required equivalent imperfections for use in the out-of-plane stability design of beams by second-order inelastic analysis (i.e. GMNIA) can be calibrated, are generated. The benchmark data were obtained following the recommendations set out in [9, 10, 11], featuring the GMNIA of beam FE models with geometric imperfections, residual stresses and strain limits to simulate cross-section failure. The key components of the procedure followed to obtain the benchmark data, including validation against physical experiments, are described in this section.

*3.1 Modelling approach*

The finite element analysis software Abaqus [31] was used to carry out the GMNIA simulations. The shear deformable prismatic Timoshenko beam element referred to as B31OS in Abaqus [31], which allows for the effects of torsion and warping in open-sections, was used [32-34]. Fork-end support conditions, allowing warping deformations (by not restraining the 7th degree of freedom [31]) but fully restraining twisting at the supports, were employed for all members.

The investigations carried out in this section cover: (i) different grades of hot-rolled steel (S235, S355 and S420) and stainless steel (austenitic, duplex and ferritic) members, (ii) different ratios of the major axis bending moments applied at the beam ends $\psi$ = 1, 0.5, 0, -0.5 and -1, (iii) a range of normalised LTB slenderness values $\bar{\lambda}_{LT}$ = 0.4, 0.6, 0.8, 1.0, 1.2 and 1.4, and (iv) a series of different cross-section geometries – European HEB 100, HEB 400, HEB 700, HEB 1000, IPE 100, IPE 140, HEM 200, HEA 100, HEA 800 profiles – covering a range of cross-section slenderness values $\bar{\lambda}_p$ (see Section 3.4) between 0.14 and 0.48. Note that the influence of the fillet radii was not included in either the benchmark models described in this section or the design models described in later sections. Beams with closed cross-sections, such as square or circular hollow sections, are not generally vulnerable to LTB [35], and thus were not assessed in this study.

*3.2 Material modelling*

Hot-rolled steel and stainless steel have distinctively different material characteristics. While hot-rolled steel has an elastic stage with a clear yield point, followed by a plateau and then a strain hardening region, stainless steel is characterised by a rounded stress-strain response with no clear yield point and significant strain hardening. The material parameters adopted in this study are summarised in Table 3. The Poisson's ratio was taken as $\nu$ = 0.3 in the elastic range and $\nu$ = 0.5 in the plastic range. For hot-rolled steel, the three steel grades, S235, S355 and

S420, were considered. The quad-linear stress-strain model, developed by Yun and Gardner [36] and included in prEN 1993-1-14 [37], was used in this study, as illustrated in Fig. 4 (a). The three input parameters for the material model are the Young's modulus $E$, yield stress $f_y$ and ultimate stress $f_u$. The stress-strain ($\sigma$-$\varepsilon$) relationship over the full range is defined by:

$$\sigma = \begin{cases} E\varepsilon & \text{for } \varepsilon \le \varepsilon_y \\ f_y & \text{for } \varepsilon_y < \varepsilon \le \varepsilon_{sh} \\ f_y + E_{sh}\left(\varepsilon - \varepsilon_{sh}\right) & \text{for } \varepsilon_{sh} < \varepsilon \le C_1\varepsilon_u \\ f_{C_1\varepsilon_u} + \dfrac{f_u - f_{C_1\varepsilon_u}}{\varepsilon_u - C_1\varepsilon_u}\left(\varepsilon - C_1\varepsilon_u\right) & \text{for } C_1\varepsilon_u < \varepsilon \le \varepsilon_u \end{cases} \tag{20}$$

where the strain hardening strain $\varepsilon_{sh}$ is given by:

$$\varepsilon_{sh} = 0.1\frac{f_y}{f_u} - 0.055 \qquad \text{but } 0.015 \le \varepsilon_{sh} \le 0.03 \tag{21}$$

the ultimate strain $\varepsilon_u$ is determined from:

$$\varepsilon_u = 0.6\left(1 - \frac{f_y}{f_u}\right) \qquad \text{but } \varepsilon_u \ge 0.06 \tag{22}$$

and the strain hardening modulus $E_{sh}$ is determined from:

$$E_{sh} = \frac{f_u - f_y}{C_2\varepsilon_u - \varepsilon_{sh}} \tag{23}$$

The constants $C_1$ and $C_2$ are given by Eqs. (24) and (25), respectively.

$$C_1 = \frac{\varepsilon_{sh} + 0.25\left(\varepsilon_u - \varepsilon_{sh}\right)}{\varepsilon_u} \tag{24}$$

$$C_2 = \frac{\varepsilon_{sh} + 0.4\left(\varepsilon_u - \varepsilon_{sh}\right)}{\varepsilon_u} \tag{25}$$

For stainless steel, three families – austenitic (A), duplex (D) and ferritic (F) – were considered; for each family, one typical grade was chosen. The standardised material properties for numerical studies defined by Afshan et al. [38] were employed, as listed in Table 3. The two-stage Ramberg-Osgood material model [39-41] was used in this study, as given by Eqs. (26)-(27) and illustrated in Fig. 4 (b), where $f_y$ is the yield stress, taken as 0.2% proof stress, $\varepsilon_{0.2}$ is

the total strain at the yield stress $f_y$, equal to $0.002+f_y/E$, $E_y$ is the tangent modulus at the 0.2% proof stress, as given by Eq. (28) and $n$ and $m$ are the strain hardening exponents.

$$\varepsilon = \frac{\sigma}{E} + 0.002\left(\frac{\sigma}{f_y}\right)^n \qquad \text{for } \sigma \le f_y \tag{26}$$

$$\varepsilon = \varepsilon_{0.2} + \frac{\sigma - f_y}{E_y} + \left(\varepsilon_u - \varepsilon_{0.2} - \frac{f_u - f_y}{E_y}\right)\left(\frac{\sigma - f_y}{f_u - f_y}\right)^m \qquad \text{for } f_y < \sigma \le f_u \tag{27}$$

$$E_y = \frac{E}{1 + 0.002n\dfrac{E}{f_y}} \tag{28}$$

*3.3 Geometric imperfections and residual stresses*

Equivalent imperfections applied in a shape of single lateral bow have been shown to be unsuitable for use in loading cases with a low proportion of bending moment at midspan (e.g. antisymmetric bending) [23]. Therefore, initial geometric imperfections in the form of the first LTB eigenmode, scaled to 1/1000 of the unbraced member lengths $L$ were defined in the benchmark FE models. In this study, initial twist imperfections were not included in the beam FE models; this is deemed suitable since initial twist imperfections have been shown to have negligible influence on the ultimate lateral-torsional buckling resistances of beams [18, 42] and are stated to not generally be needed in EN 1993-1-1 [1]. Residual stresses were also introduced into the FE models. Residual stress patterns in carbon steel and stainless steel sections differ due to the different mechanical and thermal properties resulting from the specific chemical compositions and microstructure [43]. For hot-rolled carbon steel, the residual stress pattern given by ECCS [20] was utilised, as illustrated in Fig. 5 (a). For stainless steel, the residual stress pattern for welded I-sections developed by Yuan et al. [44] was adopted, as illustrated in Fig. 5 (b). The residual stresses were introduced into the beam FE models using the SIGINI user subroutine [31], by defining the initial stresses at section points prior to the loading step. To accurately represent the residual stress distributions, each web and flange plate was assigned

33 section points for the hot-rolled steel profiles [45] and 41 sections points for the stainless steel profiles [46] along the width, respectively. Corresponding plastic strains due to the residual stresses [47] were also assigned in the case of the stainless steel models using the HARDINI user subroutine [31]. Note that it was not necessary to include such plastic strains in the steel profiles since the imposed residual stress remained in the elastic range of the material.

*3.4 Continuous strength method (CSM)*

Cross-section failure was signified in the developed FE models by the maximum compressive strain reaching the CSM strain limit $\varepsilon_{\mathrm{csm}}$, as given by Eqs. (29) and (30) for hot-rolled carbon steel [48-51]:

$$\frac{\varepsilon_{\mathrm{csm}}}{\varepsilon_{\mathrm{y}}} = \frac{0.25}{\bar{\lambda}_{\mathrm{p}}^{\,3.6}} \quad \text{but } \leq \Omega \quad \text{for } \bar{\lambda}_{\mathrm{p}} \leq 0.68 \tag{29}$$

$$\frac{\varepsilon_{\mathrm{csm}}}{\varepsilon_{\mathrm{y}}} = \left(1 - \frac{0.222}{\bar{\lambda}_{\mathrm{p}}^{\,1.05}}\right)\frac{1}{\bar{\lambda}_{\mathrm{p}}^{\,1.05}} \quad \text{for } 0.68 < \bar{\lambda}_{\mathrm{p}} \leq 1.0 \tag{30}$$

and Eqs. (31) and (32) for materials exhibiting a rounded stress-strain response, including stainless steel [39], aluminium alloys [52] and cold-formed steel [53].

$$\frac{\varepsilon_{\mathrm{csm}}}{\varepsilon_{\mathrm{y}}} = \frac{0.25}{\bar{\lambda}_{\mathrm{p}}^{\,3.6}} + \frac{0.002}{\varepsilon_{\mathrm{y}}} \quad \text{but } \leq \Omega \quad \text{for } \bar{\lambda}_{\mathrm{p}} \leq 0.68 \tag{31}$$

$$\frac{\varepsilon_{\mathrm{csm}}}{\varepsilon_{\mathrm{y}}} = \left(1 - \frac{0.222}{\bar{\lambda}_{\mathrm{p}}^{\,1.05}}\right)\frac{1}{\bar{\lambda}_{\mathrm{p}}^{\,1.05}} + \frac{0.002\left(\sigma_{\mathrm{Ed,max}} / f_{\mathrm{y}}\right)^{n}}{\varepsilon_{\mathrm{y}}} \quad \text{for } 0.68 < \bar{\lambda}_{\mathrm{p}} \leq 1.0 \tag{32}$$

In Eqs. (29)-(32), which are referred to as the base curves in the continuous strength method (CSM), $\varepsilon_{\mathrm{csm}}$ is the maximum strain that a cross-section can endure prior to failure, $\varepsilon_{\mathrm{y}} = f_{\mathrm{y}}/E$ is the yield strain, $\Omega$ is a project specific design parameter that defines an upper bound to the maximum permitted strain, for which the value of 15 is recommended [10], $\sigma_{\mathrm{Ed,max}}$ is the

maximum stress in the cross-section and $\bar{\lambda}_{\mathrm{p}}$ is the cross-section slenderness, determined from Eq. (33):

$$\bar{\lambda}_{\mathrm{p}} = \sqrt{\frac{f_{\mathrm{y}}}{\sigma_{\mathrm{cr,cs}}}} \tag{33}$$

where $\sigma_{\mathrm{cr,cs}}$ is the elastic local buckling stress of the full cross-section which can be calculated numerically (e.g. through the finite strip software *CUFSM* [54]), or using the equations developed by Gardner et al. [55]; the latter approach is adopted in this study.

*3.5 Generation of benchmark data*

Beam finite elements are able to directly capture global member instabilities, such as LTB, but are unable to capture local cross-section instabilities. Thus, in [10, 56], it was proposed that the CSM strain limits are applied to capture cross-section failure, by checking the maximum compressive longitudinal strains against the corresponding CSM strain limits for all cross-sections in the structure at each load increment. Note that the strain limit is applied only to the strains resulting from the applied load (i.e. not the strains arising from the residual stresses). In the developed method, a GMNIA of the structure using beam finite elements is first performed; the ultimate capacity is then defined based on either (i) the peak load factor obtained from the analysis or (ii) the load factor at which the CSM strain limit is attained at any cross-section in the considered member or structure, whichever occurs first [46]. The accuracy and reliability of this approach have been verified for carbon steel [10, 45, 51, 57] and stainless steel structures [11], considering a wide range of cases. Relative to the traditional design calculations, this design method provides more accurate and consistent member capacity predictions, removing the need for cross-section classification, individual member buckling checks and the calculation of effective lengths in the determination of member resistances [45].

To take account of the beneficial influence of local strain gradients along the member lengths on cross-section resistance, it was recommended in [10] to average the maximum compressive

longitudinal strains in the cross-sections over a defined length. To enable the application of the strain averaging approach [10], the lengths of the beam elements were taken as less than or equal to the corresponding elastic local buckling half-wavelengths $L_{b,cs}$ of the cross-sections, which can be obtained numerically, e.g. through the finite strip software *CUFSM* [54], or through the expressions presented in [58], which were adopted in the present study. In this study, 100 beam elements were used to model each member, to accurately capture the spread of plasticity, as adopted in the previous similar studies [46,59].

### *3.6 Validation of beam FE models*

Although the aforementioned beam FE modelling approach has been successfully employed in numerous previous investigations [10, 11, 13, 45, 57], in the present study, prior to being used to generate benchmark data, the approach is further validated against the results from 44 experiments reported in the literature [60-65], focusing on beams experiencing LTB. The loading configurations included (i) 3-point bending and 4-point bending [60], (ii) 3-point bending with eccentrically applied vertical loading, leading to additional torsion [61-64] and (iii) concentrated loading applied at the free-end of cantilever beams [65]. The boundary and loading conditions of the beam FE models were consistent with those employed in the tests. The measured global geometric imperfection amplitudes and residual stresses were incorporated into the FE models where reported; the shape of the geometric imperfections were defined as the first LTB eigenmode. If no measured imperfection amplitudes or residual stresses were provided, the values from Section 3.3 were employed. The results of the validation study, including the mean and coefficient of variation (CoV) values of the ratios of the ultimate resistances obtained from beam FE models $\alpha_{u,FE}$ to those obtained in the experiments $\alpha_{u,test}$ (i.e. $\alpha_{u,FE}/\alpha_{u,test}$), are summarised in Table 4. It can be seen that the beam FE models developed in this study are able to provide ultimate strength predictions that are consistently very close to experimental results.

In Fig. 6, the experimental and numerical load-twist and load-vertical displacement curves for a sample of beams tested under eccentric 3-point bending in [62, 63] and [64] are shown, where $P$ is the applied load, $\phi$ and $w$ are the twist and vertical displacement at midspan, respectively, and $P_{\mathrm{u,test}}$ is the ultimate load obtained from the experiments. It can be seen from the figures that the beam FE models accurately capture the load-deformation response observed in the experiments, and are therefore considered to be suitable for the generation of benchmark data, against which the required equivalent imperfections can be determined.

## 4. REQUIRED EQUIVALENT IMPERFECTIONS FOR DESIGN BY SECOND-ORDER INELASTIC ANALYSIS

In this section, the required equivalent imperfections for use in the out-of-plane stability design of steel members by second-order inelastic analysis are calculated by iteratively running beam FE models with varying initial imperfection amplitude $e_0$ until the obtained ultimate member resistance coincides with the benchmark data to within 0.5%. This is illustrated in Fig. 7 for two example beams under uniform bending. The beam FE models used to back-calculate the required equivalent imperfections were developed following the same approach as the benchmark FE models except with a varying amplitude of geometric imperfection and no residual stresses.

It should be noted that the required equivalent imperfections calculated herein were introduced into the FE models through the scaling of the first LTB eigenmode, as employed in the benchmark FE models. The equivalent imperfection applied in a shape of single lateral bow has been shown to be unsuitable for use in loading cases with a low proportion of bending moment at midspan (e.g. antisymmetric bending) [23]. A similar conclusion was reached in the study of Ebel [66] in which the shape of the first LTB eigenmode was recommended for

equivalent imperfections. The new design curves for LTB in prEN 1993-1-1 [12] (see Section 2.2) were also developed based on imperfections in the shape of the first LTB eigenmode [7].

The amplitude of the geometric imperfections introduced into benchmark FE models was equal to $L/1000$. Since the equivalent imperfections take account of the combined effects of geometric imperfections and residual stresses, the required values $e_{0,\mathrm{req}}$ must be larger than $L/1000$. Fig. 7 (a) and (b) show the required equivalent geometric imperfection amplitudes $e_{0,\mathrm{req}}$ for two S355 hot-rolled steel members subjected to uniform bending $M$, with HEB 400 and HEA 100 cross-sections, respectively, and $\bar{\lambda}_{\mathrm{LT}} = 1.2$. It can be seen that the HEA 100 cross-section, which has a depth-to-width ratio $h/b$ less than 1.2, needs a higher required equivalent imperfection than that of the member with the HEB 400 cross-section (i.e. $L/360 > L/600$), where $h/b$ is greater than 1.2. This is because, as shown in Fig. 5 (a), for hot-rolled steel I-section members, larger residual stresses exist in cross-sections with $h/b \leq 1.2$ than with $h/b > 1.2$, resulting in a more detrimental effect on member resistances, and consequently requiring larger equivalent imperfection amplitudes. This is also reflected in the upcoming prEN 1993-1-1 [12], which includes a higher LTB imperfection factor $\alpha_{\mathrm{LT}}$ for the LTB curves of cross-sections with $h/b \leq 1.2$.

Figs. 8 and 9 show the required values of the non-dimensional equivalent imperfections $j_{\mathrm{req}} = L / e_{0,\mathrm{req}}$ for hot-rolled and stainless steel members, respectively, subjected to a range of bending moment distributions along the member length ($\psi$ = 1, 0.5, 0, -0.5 and -1), achieved through varying the ratio of the applied end moments (i.e. $\psi = M_2/M_1$, where $M_1$ and $M_2$ are the bending moments applied at each end of the beam) versus member slenderness $\bar{\lambda}_{\mathrm{LT}}$. It should be noted that members with different member slenderness have varying sensitivity to geometric imperfections. This is illustrated in Fig. 10, which shows the ratio of ultimate load carrying capacities obtained from GMNIA with CSM strain limits $M_{\mathrm{u}}$, with varying non-dimensional geometric imperfection values $j = L/e_0$ ranging from 100 to 1000, to the benchmark results $M_{\mathrm{FE}}$,

for two hot-rolled steel HEB 400 members with member slenderness $\bar{\lambda}_{LT}$ = 0.4 and 1.0, respectively, subjected to uniform bending $M$. It can be observed that the more slender member (with $\bar{\lambda}_{LT}$ = 1.0), for which LTB is more pronounced, is more sensitive to the geometric imperfections. It can be seen that with decreasing geometric imperfection amplitude, there is a clear increase in ultimate resistances. By contrast, the stockier member (with $\bar{\lambda}_{LT}$ = 0.4) is much less sensitive to geometric imperfections; when the imperfection $e_0$ varies from $L$/100 to $L$/1000, the difference between the ultimate bending moment resistances is less than 10%. In the range of $L/1000 \leq e_0 \leq L/500$, the ultimate resistances are almost constant and all are within 0.5% of the benchmark results. This confirms that for stocky members, variation in the initial geometric imperfection has little influence on the ultimate resistance.

In this study, as in [13], it is proposed that the imperfection factor is incorporated into the definition of the equivalent imperfection amplitude $e_{0,LT}$, to capture the varying influence of residual stresses for different cross-section types. Since the influence of geometric properties is directly captured by GMNIA using three-dimensional beam finite elements, the employed imperfection factor does not require inclusion of the geometric parameter $\sqrt{W_{el,y} / W_{el,z}}$ discussed in Section 2.2, and is proposed to be simply taken as $\alpha_z$ (i.e. the imperfection factor for minor axis flexural buckling), as given in Table 5, which generally corresponds to the upper limit of $\alpha_{LT}$ provided in prEN 1993-1-1 [12] and prEN 1993-1-4 [14]. This ensures that the severity of the influence of residual stresses is captured, but without inheriting the additional compensatory effects included in $\alpha_{LT}$ for calibration of the LTB curves.

Both Eqs. (17) and (19) include the material parameter $\varepsilon$, to allow for the influence of material yield strength on the required equivalent imperfections in GNIA. However, since the influence of the material nonlinearity is directly captured by GMNIA, the equivalent imperfections for

LTB design are no longer required to be a function of $\varepsilon$. This mirrors the provisions in [13] for flexural buckling design by GMNIA.

Hence, adopting the same format of the expressions for flexural buckling [13], the equivalent imperfections proposed in this study are a function of the imperfection factor $\alpha_z$ and a reference relative imperfection $\beta_{LT}$, as given by Eq. (34), where $\alpha_z$ is determined from Table 5.

$$e_{0,LT} = \alpha_z \beta_{LT} L \tag{34}$$

Based on the back-calculated required equivalent imperfections $e_{0,req}$, the required values of the reference relative imperfection $\beta_{req}$ can be determined as:

$$\beta_{req} = e_{0,req} / \alpha_z L \tag{35}$$

Figs. 11 and 12 show the $\beta_{req}$ values for hot-rolled steel and stainless steel members, respectively, for a range of cross-sections, member slenderness values and bending moment gradients. With the introduction of the imperfection factor $\alpha_z$, the required values of $1/\beta_{req}$ are less scattered than the required values of $j_{req} = L/e_{0,req}$, as shown in Figs. 8 and 9. This confirms the validity of including the imperfection factor $\alpha_z$ in the definition of $e_{0,LT}$.

## 5. DESIGN RECOMMENDATIONS AND EVALUATION

In this section, recommendations are made for equivalent imperfections for use in the out-of-plane stability design of steel and stainless steel members by GMNIA. Two proposals for equivalent imperfection amplitudes are made for: (1) the scaling of the first LTB eigenmode, denoted $e_{0,mod}$ and (2) for direct modelling of lateral bow imperfection shapes, denoted $e_{0,bow}$. The ultimate strength predictions obtained through the use of the recommended equivalent imperfections are compared against both the benchmark FE results and Eurocode calculated resistances. The reliability of the recommendations is then assessed, and their application is demonstrated through worked examples. Note that in the present study, CSM strain limits are applied to capture cross-section failure, but cross-section checks can alternatively and

conservatively be used. Nevertheless, the developed equivalent imperfections are independent of the slenderness and classification of the cross-section.

### *5.1 Design recommendations*

#### *5.1.1 Mode imperfection $e_{0,\mathrm{mod}}$*

Based on the required imperfections determined in Section 4 and shown in Figs. 11 and 12, the reference relative imperfection value of $\beta_{\mathrm{LT}}$ = 1/150 is proposed for use in LTB design by GMNIA of members subjected to different bending moment gradients, for both hot-rolled steel and stainless steel, and for all the member slenderness values and cross-sections examined herein, as given by Eq. (36).

$$e_{0,\mathrm{mod}} = \alpha_{\mathrm{z}} \beta_{\mathrm{LT}} L = \alpha_{\mathrm{z}} L / 150 \tag{36}$$

A singe value of $\beta_{\mathrm{LT}}$ is chosen for all cases, independent of the member slenderness $\bar{\lambda}_{\mathrm{LT}}$, in order to retain simplicity. A certain level of conservatism is therefore accepted for some geometries [13, 29], as indicated in Section 4.

It can be seen in Figs. 11 and 12 that the proposed recommendation of $\beta_{\mathrm{LT}}$ = 1/150 provides a safe-sided approximation to the majority of the required values of $\beta_{\mathrm{req}}$. This value is also consistent with that provided in [13] for use in flexural buckling design by GMNIA; in both studies, the structural response and influence of varying geometric characteristics and material properties is directly captured in the GMNIA and the influence of different residual stresses is captured through the imperfection factor ($\alpha$ or $\alpha_{\mathrm{z}}$).

#### *5.1.2 Lateral bow imperfection $e_{0,\mathrm{bow}}$*

The proposed equivalent imperfection detailed above is recommended for use with the first LTB eigenmode. However, in practical design situations, it is somewhat cumbersome to conduct a linear buckling analysis (LBA) prior to GMNIA to obtain the LTB eigenmode; furthermore, the appropriate isolation of members within a structure and the choice of

eigenmode is not always straightforward. Therefore, an alternative design recommendation, whereby equivalent imperfections are applied through direct modelling as lateral bow imperfections of amplitude $e_{0,\mathrm{bow}}$, is also made herein. As mentioned in Section 4, an imperfection in the shape of a half-sine wave is unsuitable for bending moment diagrams with a low proportion of bending moment at midspan [23]. Hence, to cover the range of possible bending moment diagrams, a combination of two shapes of lateral imperfections is proposed in this study: (1) a half-sine wave, which is similar to the deformed shape of members under uniform bending ($\psi$ = 1), and (2) a full-sine wave, corresponding to the deformation profile of members under antisymmetric bending ($\psi$ = -1). The amplitude of the full-sine wave imperfection is taken as $\alpha_z L/215$, which is approximately equal to 70% of that of the half-sine wave imperfection. Hence, a lateral equivalent bow imperfection $e_{0,\mathrm{bow}}$ is defined as the summation of a half-sine wave with imperfection amplitude $e_{0,\mathrm{bow},1}$ (with $\beta_{\mathrm{LT},1} = 1/150$), as determined from Eq. (37), and a full-sine wave with imperfection amplitude $e_{0,\mathrm{bow},2}$ (with $\beta_{\mathrm{LT},2} = 1/215$), as determined from Eq. (38). This proposal is illustrated in Fig. 13, and given in Table 6.

$$e_{0,\mathrm{bow},1} = \alpha_z \beta_{\mathrm{LT},1} L = \alpha_z L / 150 \tag{37}$$

$$e_{0,\mathrm{bow},2} = \alpha_z \beta_{\mathrm{LT},2} L = \alpha_z L / 215 \tag{38}$$

Note that the amplitude of the half-sine wave bow imperfection is consistent with that for flexural buckling [13]. Note also that the summation of these two imperfections is not symmetric, and thus should be applied in practice in the most unfavourable direction and form.

*5.2 Evaluation of design recommendations*

The proposed mode $e_{0,\mathrm{mod}}$ and lateral bow $e_{0,\mathrm{bow}}$ equivalent imperfections are assessed in this section for application with GMNIA. The assessment was carried out on 1134 steel members and 1134 stainless steel members, each considering three material grades, nine cross-sections,

six member slenderness values, the seven load cases indicated in Section 3.1, as well as the load cases of uniformly distributed loading (UDL) and a concentrated central point load.

*5.2.1 Mode imperfection* $e_{0,\mathrm{mod}}$

Fig. 14 shows comparisons of the ultimate resistance predictions obtained from (1) the proposed design approach $M_{\mathrm{mod}}$ using GMNIA with the eigenmode shape of equivalent imperfection and $e_{0,\mathrm{mod}}$, (2) the prEN 1993-1-1 [12] LTB curves $M_{\mathrm{EC3}}$ and (3) the benchmark FE models (GMNIA with eigenmode imperfections of amplitude $L/1000$ plus residual stresses) $M_{\mathrm{FE}}$, for the examined hot-rolled steel members subjected to different loading conditions. The mean values of the member resistance predictions obtained using the different design approaches relative to the benchmark FE results are summarised in Table 7. It can be seen that the Eurocode predictions are overly conservative for slender members (e.g. $\bar{\lambda}_{\mathrm{LT}} \geq 1.2$); this is because the "post-critical" load-carrying mechanism in slender members (see Section 2.3.1.2) was not allowed for in the derivation of the buckling curves provided in prEN 1993-1-1 [12]. For some stocky members ($\bar{\lambda}_{\mathrm{LT}} = 0.4$), the Eurocode predictions lie slightly on the unsafe side. The resistance predictions obtained from design by GMNIA using the proposed equivalent imperfections are more accurate and less scattered than those obtained using the Eurocode 3 buckling curves. The large majority of the predictions obtained using the proposed equivalent imperfections are safe-sided (i.e. $M_{\mathrm{mod}}/M_{\mathrm{FE}} \leq 1$). For stainless steel members, similar conclusions can also be made, as shown in Fig. 15. Compared with the design method in prEN 1993-1-4 [14], design by GMNIA employing the proposed equivalent mode imperfections $e_{0,\mathrm{mod}}$ provides more accurate member resistance predictions while remaining safe-sided. Note that initial twist was not introduced into the beam FE models in this study, as explained in Section 3.3.

*5.2.2 Lateral bow imperfection $e_{0,bow}$*

The proposal for the lateral bow equivalent imperfection $e_{0,bow}$ was assessed in the same manner as above. Figs. 16 and 17 show comparisons of the ultimate resistance predictions obtained from (1) GMNIA with the proposed lateral bow equivalent imperfection $M_{bow}$, (2) the prEN 1993-1-1 LTB curves $M_{EC3}$ and the benchmark FE models $M_{FE}$, for hot-rolled steel and stainless steel members, respectively, subjected to different loading conditions. Comparing the results presented in Figs. 14-17 and Table 7, it can be seen that, in general, for both steel and stainless steel members, the mode equivalent imperfection provides the most accurate resistance predictions. The lateral bow imperfection provides more conservative resistance predictions in the cases where $\psi$ = 0 and -0.5; in these cases, the shape of the applied combined lateral bow imperfections is similar to the LTB eigenmodes but the bow equivalent imperfection amplitude $e_{0,bow}$ is more severe than $e_{0,mod}$. Nonetheless, employing the lateral bow imperfection in GMNIA provides very good results, with more accurate predictions than the Eurocode design calculations, and with the benefit of not requiring an LBA for obtaining the LTB eigenmode.

*5.3 Reliability analysis*

The reliability and required partial safety factor $\gamma_{M1}^{*}$ for the proposed equivalent imperfections for use in design by GMNIA were evaluated through the first order reliability method (FORM) set out in EN 1990:2002 [67] and further explained by Afshan et al. [68]. According to EN 1990:2002 [67], typical buildings fall into reliability class RC2 with a 50-year design life and a target reliability index of 3.8 for ultimate limit state design. The derivation of partial safety factors are based on this value. The recommended values of the partial safety factors $\gamma_{M1}$ are 1.0 for steel in prEN 1993-1-1 [12] and 1.1 for stainless steel in prEN 1993-1-4 [14].

The ultimate bending moment capacities of members experiencing LTB are dependent on the basic variables – yield stress $f_y$, major axis plastic section modulus $W_{pl,y}$ and Young's modulus

$E$. The influence of these variables change with the member proportions for each numerical simulation. The dependency of the member resistance on the basic variables $f_y$, $W_{pl,y}$ and $E$ can be derived for each numerical simulation following the method set out in [68], presented as the exponents $c$, $d$ and $e$ to be applied to the basic variables (i.e. $f_y^c$, $W_{pl,y}^d$, $E^e$), as given by Eqs. (39), (40) and (41), respectively, where $M_{1.05fy}$, $M_{1.05Wpl,y}$ and $M_{1.05E}$ are the ultimate bending moment capacities obtained from the numerical analysis with the yield stress multiplied by 1.05, with the major axis plastic section modulus multiplied by 1.05 and with the Young's modulus multiplied by 1.05, respectively, and $M_{fy}$, $M_{Wpl,y}$ and $M_E$ are the original ultimate bending moment capacities.

$$c = \frac{\ln\left(M_{1.05fy} / M_{fy}\right)}{\ln\left(1.05 f_y / f_y\right)} \tag{39}$$

$$d = \frac{\ln\left(M_{1.05Wpl,y} / M_{Wpl,y}\right)}{\ln\left(1.05 W_{pl,y} / W_{pl,y}\right)} \tag{40}$$

$$e = \frac{\ln\left(M_{1.05E} / M_E\right)}{\ln\left(1.05 E / E\right)} \tag{41}$$

Fig. 18 shows values of the exponents $c$, $d$ and $e$ obtained for members subjected to uniform bending. Fig. 18 (a) shows the values obtained using the proposed mode equivalent imperfections $e_{0,mod}$ for the considered hot-rolled steel members, while Fig. 18 (b) shows the values obtained using the proposed lateral bow equivalent imperfections $e_{0,bow}$ for the considered stainless steel members. In general, with increasing member slenderness $\bar{\lambda}_{LT}$, the dependency on the yield stress $f_y$ (represented by exponent $c$) decreases, while the dependency on the major axis plastic section modulus $W_{pl,y}$ (represented by exponent $d$) and the Young's modulus (represented by exponent $e$) increases. This reflects the transition from in-plane bending, dominated by plasticity to elastic buckling, controlled by Young's modulus, with increasing slenderness, together with a general dependency on the section geometry. However, it can be seen from Fig. 18 that there are a few outliers (highlighted in red dashed circles) not

consistent with the above statements. These are due to the "post-critical" load-carrying mechanism mentioned in Section 2.3.1.2: the ultimate resistance of slender members can exceed the elastic critical buckling moment $M_{cr}$ and approach the minor axis bending resistance. Hence, for these slender members, the dependencies on the yield stress and geometric properties (presented by exponents $c$ and $d$) approach unity, while the dependency on the Young's modulus (presented by exponent $e$) reduces.

The adopted values of material overstrength $f_{y,mean}/f_{y,nom}$ (i.e. the ratio of mean to nominal yield strength) and the CoV of yield strength $V_{fy}$ were specified according to prEN 1993-1-1 [12] for steel and reference [69] for stainless steel; the CoV of geometric properties $V_{Wpl,y}$ was determined according to [68]; the CoV of Young's modulus $V_E$ was taken as 0.03 for both materials [12]. The values assumed herein are listed in Tables 8 and 9. The combined coefficient of variation $V_{rt}$ of the material and geometric basic variables is given by Eq. (42) [70]; note that $V_{rt}$ is calculated for each numerical simulation.

$$V_{rt} = \sqrt{\left(cV_{fy}\right)^2 + \left(dV_{Wpl,y}\right)^2 + \left(eV_E\right)^2} \tag{42}$$

It should be noted that, as recommended in [11, 13], in the implementation of the design method through second-order inelastic analysis (i.e. GMNIA), the Young's modulus $E$ should be taken as a reduced (characteristic) value, rather than the mean value. Hence, in this study, the reduced values of $E$ = 200,000 N/mm$^2$ for steel and $E$ = 191,000 N/mm$^2$ for stainless steel were adopted [12-14, 37] in the performed GMNIA design calculations.

The mean correction factor $b$ was calculated using a modified definition based on the average ratio of the benchmark resistance $r_e$ to the predicted resistance $r_t$, as given by Eq. (43), instead of the least-squares method recommended in EN 1990:2002 [67]. This prevents the derived value of $b$ from being biased toward the data points with higher resistance values [70, 71].

$$b = \frac{1}{n}\sum_{i=1}^{n}\frac{r_{\mathrm{e,i}}}{r_{\mathrm{t,i}}} \tag{43}$$

The key reliability analysis results for all considered cases are reported in Tables 8 and 9, including the mean correction factor $b$, the coefficient of variation of the results obtained using the proposals relative to the benchmark FE results $V_\delta$ and the required value of partial safety factor $\gamma_{M1}^*$. All values of $b$ are greater than 1, indicating the mean predictions obtained using two proposals are safe-sided; this is shown in Table 7. The required values of the partial safety factor $\gamma_{M1}^*$ are slightly higher than the target values of 1.0 for steel members [12] and generally lower than 1.1 for stainless steel members [14], but all are in line with the recommendations given by SAFEBRICTILE [72, 73], which allows a small exceedance of the target values to allow for the influence of the combined coefficient of variation $V_r$ incorporating the variability of the model and the basic variables. Note that if the values of $f_{y,mean}/f_{y,nom}$ and $V_{fy}$ are taken as 1.30 and 0.060 instead of 1.20 and 0.050 for austenitic stainless steel and taken as 1.20 and 0.045 instead of 1.15 and 0.055 for ferritic stainless steel (as assumed in the reliability analyses performed in [68]), the calculated values of $\gamma_{M1}^*$ still satisfy the SAFEBRICTILE [72, 73] requirements. Therefore, the two proposals for equivalent imperfections are deemed to be suitable for use in the out-of-plane stability design of steel and stainless steel members by GMNIA, in conjunction with the recommended values of the partial safety factor $\gamma_{M1}$ i.e. 1.0 for steel and 1.1 for stainless steel.

*5.4 Worked examples*

Two worked examples are presented in this section to illustrate the implementation of the proposed equivalent imperfections in design by second-order inelastic analysis.

The first worked example considers a beam made of grade S355 steel ($f_y$ = 355 MPa, $f_u$ = 510 MPa, reduced value of $E$ = 200,000 N/mm$^2$ and $\nu$ = 0.3) with a hot-rolled HEA 100 cross-section and a length of $L$ = 4685 mm, which corresponds to a relative LTB member slenderness

$\bar{\lambda}_{LT}$ = 1.2; the considered beam is subjected to uniform major axis bending moment $M$, as shown in Fig. 19 (a).

The second worked example considers a beam made of duplex stainless steel ($f_y$ = 530 MPa, $f_u$ = 770 MPa, $n$ = 9.3, $m$ = 3.6, reduced value of $E$ = 191,000 N/mm$^2$ and $\nu$ = 0.3) with a cross-section equivalent to an HEB 100 and a length of $L$ = 5690 mm, which corresponds to a relative LTB member slenderness $\bar{\lambda}_{LT}$ = 1.3; the considered beam is subjected to a concentrated central point load $P$, generating an internal major axis bending moment $M$ at midspan, as shown in Fig. 19 (b).

Fig. 19 (a) shows the normalised applied bending moment for worked example 1 versus lateral displacement paths of the considered beams, as well as the resulting ultimate load predictions obtained from: (1) GMNIA with $e_0 = L/1000$ + residual stress (R.S.), i.e. the benchmark FE result, (2) GMNIA with $e_0 = e_{0,mod}$, (3) GMNIA with $e_0 = e_{0,bow}$, (4) GNIA with $e_0 = e_{0,LT,pl,b\text{-}c}$, (5) GNIA with $e_0 = e_{0,LT,pl,tab}$ and (6) the member buckling check given in prEN 1993-1-1 [12] (see Section 2.2) $M_{EC3}$. The corresponding graph and ultimate load predictions for worked example 2, with the normalised internal major axis bending moment at midspan (i.e. $M/M_{pl,y}$) plotted on the vertical axis, is shown in Fig. 19 (b). A summary of the results is given in Table 10.

Considering the first worked example, the prediction obtained from GNIA using the back-calculated equivalent imperfection $e_{0,LT,pl,b\text{-}c}$ with a linear plastic cross-section check is located on the unsafe side of the benchmark result and overpredicts the resistance by 5%. The prediction obtained from GNIA using the tabulated equivalent imperfection $e_{0,LT,pl,tab}$ with a linear plastic cross-section check is safe-sided but overly conservative compared with the benchmark FE result $M_{FE}$, with $M_{e0,LT,pl,tab}$ = 0.909$M_{FE}$. Use of the proposed equivalent imperfections in GMNIA provides close and safe-sided predictions compared with the

benchmark FE result $M_{FE}$ with $M_{mod}/M_{FE}$ = 0.988 and $M_{bow}/M_{FE}$ = 0.973. Use of the proposed equivalent imperfections in GMNIA provides an increase in capacity of about 14%, compared to the Eurocode design prediction $M_{EC3}$ for the case considered in this worked example. The failure of this member in GMNIA was stability governed (i.e. due to the attainment of the peak load prior to the CSM strain limit being reached).

Similar observations also can be made for the second worked example. Again, use of the proposed equivalent imperfections in GMNIA provides close and safe-sided predictions compared with the benchmark FE result $M_{FE}$, with $M_{mod}/M_{FE}$ = 0.991 and $M_{bow}/M_{FE}$ = 0.993, corresponding to an increase in capacity of about 25%, 7% and 17% compared to the Eurocode design prediction $M_{EC3}$, the predictions obtained from GNIA using the back-calculated equivalent imperfections $e_{0,LT,pl,b\text{-}c}$ and the predictions obtained from GNIA using the tabulated equivalent imperfections $e_{0,LT,pl,tab}$, respectively. In this worked example, GMNIA failure was governed by the CSM strain limit. Note that in both worked examples, the member resistances obtained from GNIA using the back-calculated equivalent imperfection $e_{0,LT,pl,b\text{-}c}$ are higher than the buckling resistances $M_{EC3}$, since the "post-critical" load-carrying mechanism in slender members (see Section 2.3.1.2) was not allowed for in the development of the LTB curves provided in prEN 1993-1-1 [12].

## 6. CONCLUSIONS

Equivalent imperfections consider the combined influence of initial geometric imperfections and residual stresses. Current design specifications include recommendations for equivalent imperfection amplitudes for use in design by GNIA. However, no appropriate provisions are given for equivalent imperfections for use in design by GMNIA. In this study, calibrated against the benchmark results generated from GMNIA with both geometric imperfections and residual stresses, two shapes and corresponding amplitudes of equivalent imperfections for use

in the out-of-plane stability design of steel and stainless steel members by GMNIA have been developed: (1) the first LTB eigenmode with an amplitude $e_{0,\mathrm{mod}} = \alpha_z L/150$ and (2) a lateral bow imperfection $e_{0,\mathrm{bow}}$ combining of a half-sine wave with an amplitude $e_{0,\mathrm{bow},1} = \alpha_z L/150$ and a full-sine wave with an amplitude $e_{0,\mathrm{bow},2} = \alpha_z L/215$; accurate results are achieved with either approach. The minor axis flexural buckling imperfection factor $\alpha_z$, which is generally equal to the upper bound value on $\alpha_{\mathrm{LT}}$ in prEN 1993-1-1 [12] and prEN 1993-1-4 [14], is utilised in the proposed imperfection amplitudes to capture the adverse influence of residual stresses, but without inheriting the additional compensatory effects included in $\alpha_{\mathrm{LT}}$ for calibration of the LTB curves. In the design by GMNIA using the developed equivalent imperfections, cross-section checks or CSM strain limits can be used to capture cross-section failure; the latter more accurate approach is adopted in this study.

The accuracy and suitability of the proposed equivalent imperfections were assessed against benchmark FE results for 1134 steel I-section members and 1134 stainless steel I-section members, each considering three material grades, nine cross-sections, six member slenderness values and seven load cases. The resistance predictions obtained using GMNIA with the proposed equivalent imperfections (both $e_{0,\mathrm{mod}}$ and $e_{0,\mathrm{bow}}$) were shown to be accurate, safe-sided and less scattered than those obtained from the Eurocode lateral-torsional buckling curves. The suitability of the proposals developed herein for application to structural members of other cross-sectional shapes will be examined in future research.

The suitability of using the existing recommended values of partial safety factors (i.e. $\gamma_{\mathrm{M1}} = 1.0$ for steel members and 1.1 for stainless steel members) in conjunction with the proposed imperfections was demonstrated by reliability analysis. The proposals are due to be included in the new upcoming Eurocode for design by finite element analysis – prEN 1993-1-14 [37].

## ACKNOWLEDGEMENTS

The financial support provided by the China Scholarship Council (CSC) and Imperial College London for the first author is gratefully acknowledged.

## REFERENCES

[1] EN 1993-1-1. Eurocode 3: Design of steel structures - Part 1-1: General rules and rules for buildings. European Committee for Standardization, Brussels, 2005.

[2] EN 1993-1-4:2006 + A1: 2015. Eurocode 3 - Design of steel structures - Part 1-4: General rules - Supplementary rules for stainless steels. Brussels: CEN; 2015.

[3] T.V. Galambos, M.K. Ravindra, Load and resistance factor design criteria for steel beams, Structural Division, Civil and Environmental Engineering Department, Washington University, 1974.

[4] ECCS, Manual on stability of steel structures, Tech. Rep.; No. 22, Technical Committee 8 (TC 8) of European Convention for Constructional Steelwork (ECCS). 1976.

[5] D.A. Nethercot, N.S. Trahair, Inelastic lateral buckling of determinate beams, J. Struct. Div. ASCE 102 (4) (1976) 701-717.

[6] J.A. Yura, M.K. Ravindra, T.V. Galambos, The bending resistance of steel beams, J. Struct. Div. ASCE 104 (9) (1978) 1355-1370.

[7] A. Taras, Contribution to the Development of Consistent Stability Design Rules For Steel Members, PhD thesis, Technical University of Graz, 2010.

[8] S.G. Buonopane, B.W. Schafer, Reliability of steel frames designed with advanced analysis, J. Struct. Eng. 132 (2006) 267-276.

[9] L. Gardner, X. Yun, A. Fieber, L. Macorini, Steel Design by Advanced Analysis: Material Modeling and Strain Limits, Engineering. 5 (2019) 243-249.

[10] A. Fieber, L. Gardner, L. Macorini, Design of structural steel members by advanced inelastic analysis with strain limits, Eng. Struct. 199 (2019) 109624.

[11] F. Walport, L. Gardner, D.A. Nethercot, Design of structural stainless steel members by second order inelastic analysis with CSM strain limits, Thin-Walled Struct. 159 (2020) 107267.

[12] prEN 1993-1-1. Eurocode 3: Design of steel structures - Part 1-1: General rules and rules for buildings. 2019.

[13] F. Walport, L. Gardner, D.A. Nethercot, Equivalent bow imperfections for use in design by second order inelastic analysis, Structures. 26 (2020) 670-685.

[14] prEN 1993-1-4. Eurocode 3: Design of steel structures - Part 1-4: General rules - Supplementary rules for stainless steels. 2020.

[15] CEN/TR 1993-1-103. Eurocode 3: Design of Steel Structures - Part 1-103: Elastic Critical Buckling of Members, 2017.

[16] M.P. Byfield, D.A. Nethercot, An analysis of the true bending strength of steel beams, Proc. Inst. Civ. Eng. Struct. Build. 128 (1998) 188-197.

[17] C.M. King, Design moment resistance at $\bar{\lambda}_{LT}$ = 0.4. ECCS TC8 paper no. 2001-18, European Commission for Constructional Steelwork, Brussels, 2001.

[18] R. Greiner, G. Salzgeber, R. Ofner, New lateral-torsional buckling curves $\chi_{LT}$ – Numerical simulations and design formulae, ECCS TC8 report no. 2000-14, European Commission for Constructional Steelwork, Brussels, 2000.

[19] A. Taras, R. Greiner, New design curves for lateral-torsional buckling-Proposal based on a consistent derivation, J. Constr. Steel Res. 66 (2010) 648-663.

[20] ECCS, Ultimate Limit State Calculation of Sway Frames with Rigid Joints, Tech. Rep.; No. 33, Technical Committee 8 (TC 8) of European Convention for Constructional Steelwork (ECCS). 1984.

[21] M. Fortan, B. Rossi, Lateral Torsional Buckling of Welded Stainless-Steel I-Profile Beams: Design and Reliability, J. Struct. Eng. 146 (2020) 04020280.

[22] J. Lindner, U. Kuhlmann, A. Just, Verification of flexural buckling according to Eurocode 3 part 1-1 using bow imperfections, Steel Constr. 9 (2016) 349-362.

[23] R. Stroetmann, S. Fominow, Parameter studies on imperfections for the LTB-design of members based on EN 1993-1-1, Steel Constr. 12 (2019) 299-308.

[24] I. Vayas, J. Ermopoulos, G. Ioannidis, Design of Steel Structures to Eurocodes, 2019.

[25] H.H. Snijder, R.P. van der Aa, H. Hofmeyer, B.W.E.M. van Hove, Lateral torsional buckling design imperfections for use in non-linear FEA, Steel Constr. 11 (2018) 49-56.

[26] H.H. Snijder, R.P. Van Der Aa, H. Hofmeyer, B.W.E.M. Hove, Design imperfections for steel beam lateral torsional buckling, Proc. Int. Colloq. Stab. Ductility Steel Struct. SDSS 2016. (2016) 549-556.

[27] R.P. Van Der Aa, Numerical assessment of the design imperfections for steel beam lateral torsional buckling, Master thesis, Eindhoven University of Technology, 2015.

[28] R. Stroetmann, J. Lindner, Knicknachweise nach DIN en 1993-1-1, Stahlbau. 79 (2010) 793-808.

[29] J. Lindner, U. Kuhlmann, F. Jörg, Initial bow imperfections $e_0$ for the verification of Flexural Buckling According to Eurocode 3 Part 1-1 - additional considerations, Steel Constr. 11 (2018) 30-41.

[30] R. Kindmann, J. Beier-Tertel, Geometrische ersatzimperfektionen für das biegedrillknicken von trägern aus walzprofilen - Grundsätzliches, Stahlbau. 79 (2010) 689-697.

[31] ABAQUS. ABAQUS/standard user's manual. Version 6.17. Dassault Systemes Simulia Corp. USA; 2017.

[32] F. Mohri, A. Brouki, J.C. Roth, Theoretical and numerical stability analyses of unrestrained, mono-symmetric thin-walled beams, J. Constr. Steel Res. 59 (2003) 63-90.

[33] A. Sahraei, Advances in Lateral Torsional Buckling Analysis of Beam-Columns and Plane Frames, PhD thesis, University of Ottawa, 2017.

[34] A.K. Sabat, Lateral-torsional buckling analysis of steel frames with corrugated webs, Master thesis, Chalmers University of Technology, 2009.

[35] E. Ellobody, Finite element analysis and design of steel and steel-concrete composite bridges, Butterworth-Heinemann, USA (2014).

[36] X. Yun, L. Gardner, Stress-strain curves for hot-rolled steels, J. Constr. Steel Res. 133 (2017) 36-46.

[37] prEN 1993-1-14. 2019. Eurocode 3 – Design of steel structures – Part 1-14: Design by FE analysis. 2019.

[38] S. Afshan, O. Zhao, L. Gardner, Standardised material properties for numerical parametric studies of stainless steel structures and buckling curves for tubular columns, J. Constr. Steel Res. 152 (2019) 2-11.

[39] I. Arrayago, E. Real, L. Gardner, Description of stress-strain curves for stainless steel alloys, Mater. Des. 87 (2015) 540-552.

[40] E. Mirambell, E. Real, On the calculation of deflections in structural stainless steel beams: An experimental and numerical investigation, J. Constr. Steel Res. 54 (2000) 109-133.

[41] K.J.R. Rasmussen, Full-range stress-strain curves for stainless steel alloys, J. Constr. Steel Res. 59 (2003) 47-61.

[42] C. Couto, P. Vila Real, Numerical investigation on the influence of imperfections in the lateral-torsional buckling of beams with slender I-shaped welded sections, Thin-Walled Struct. 145 (2019) 106429.

[43] L. Gardner, K.T. Ng, Temperature development in structural stainless steel sections exposed to fire, Fire Saf. J. 41 (2006) 185-203.

[44] H.X. Yuan, Y.Q. Wang, Y.J. Shi, L. Gardner, Residual stress distributions in welded stainless steel sections, Thin-Walled Struct. 79 (2014) 38-51.

[45] C. Quan, M. Kucukler, L. Gardner, Design of web-tapered steel I-section members by second-order inelastic analysis with strain limits, Eng. Struct. 224 (2020) 111242.

[46] F. Walport, L. Gardner, E. Real, I. Arrayago, D.A. Nethercot, Effects of material nonlinearity on the global analysis and stability of stainless steel frames, J. Constr. Steel Res. 152 (2019) 173-182.

[47] M. Kucukler, Z. Xing, L. Gardner, Behaviour and design of stainless steel I-section columns in fire, J. Constr. Steel Res. 165 (2020) 105890.

[48] L. Gardner, The continuous strength method, Proc. Inst. Civ. Eng. Struct. Build. 161 (2008) 127-133.

[49] X. Yun, L. Gardner, N. Boissonnade, The continuous strength method for the design of hot-rolled steel cross-sections, Eng. Struct. 157 (2018) 179-191.

[50] X. Yun, L. Gardner, N. Boissonnade, Ultimate capacity of I-sections under combined loading - Part 2: Parametric studies and CSM design, J. Constr. Steel Res. 148 (2018) 265-274.

[51] A. Fieber, L. Gardner, L. Macorini, Structural steel design using second-order inelastic analysis with strain limits, J. Constr. Steel Res. 168 (2020) 105980.

[52] X. Yun, Z. Wang, L. Gardner, Full-range stress-strain curves for aluminum alloys, J. Struct. Eng. 147 (2021) 04021060.

[53] L. Gardner, X. Yun, Description of stress-strain curves for cold-formed steels, Constr. Build. Mater. 189 (2018) 527-538.

[54] Z. Li and B. W. Schafer. Buckling analysis of cold-formed steel members with general boundary conditions using CUFSM: Conventional and constrained finite strip methods. In Twentieth International Speciality Conference on Cold-Formed Steel Structures. Saint Louis, Missouri, USA, 2010.

[55] L. Gardner, A. Fieber, and L. Macorini, Formulae for calculating elastic local buckling stresses of full structural cross-sections, Structures. 17 (2019) 2-20.

[56] A. Fieber, Structural steel design using advanced analysis with strain limits, PhD thesis, Imperial College London, 2019.

[57] C. Quan, M. Kucukler, L. Gardner, Out-of-plane stability design of steel beams by second-order inelastic analysis with strain limits, Thin-Walled Struct., (in press).

[58] A. Fieber, L. Gardner, L. Macorini, Formulae for determining elastic local buckling half-wavelengths of structural steel cross-sections, J. Constr. Steel Res. 159 (2019) 493-506.

[59] M. Kucukler, L. Gardner, L. Macorini, Development and assessment of a practical stiffness reduction method for the in-plane design of steel frames, J. Constr. Steel Res. 126 (2016) 187-200.

[60] P.F. Dux, S. Kitipornchai, Inelastic beam buckling experiments, J. Constr. Steel Res. 3 (1983) 3-9.

[61] J. Lindner, T. Glitsch, Vereinfachter Nachweis für I- und U-Träger beansprucht durch doppelte Biegung und Torsion, Stahlbau. 73 (2004) 704-715.

[62] A.R. Tusnin, M. Prokic, Selection of parameters for I-beam experimental model subjected to bending and torsion, Procedia Eng. 111 (2015) 789-796.

[63] A.R. Tusnin, M. Prokic, Experimental research of I-beams under bending and torsion actions, Mag. Civ. Eng. 53 (2015) 24-31.

[64] L. Schaper, F. Jörg, R. Winkler, U. Kuhlmann, M. Knobloch, The simplified method of the equivalent compression flange: Development based on LTB tests and residual stress measurements, Steel Constr. 12 (2019) 264-277.

[65] A.L. Demirhan, H.E. Eroğlu, E.O. Mutlu, T. Yılmaz, Ö. Anil, Experimental and numerical evaluation of inelastic lateral-torsional buckling of I-section cantilevers, J. Constr. Steel Res. 168 (2020) 105991.

[66] R. Ebel, Systemabhängiges Tragverhalten und Tragfähigkeiten stabilitätsgefährdeter Stahlträger unter einachsiger Biegebeanspruchung (System-dependent bearing characteristics and load bearing capacities of steel beams under uniaxial bending), Dissertation, Ruhr-Universität Bochum, 2014.

[67] EN 1990:2002. Eurocode - Basis of structural design. Brussels, Belgium: CEN (European Committee for Standardization); 2002.

[68] S. Afshan, P. Francis, N.R. Baddoo, L. Gardner, Reliability analysis of structural stainless steel design provisions, J. Constr. Steel Res. 114 (2015) 293-304.

[69] N.R. Baddoo, F.J. Meza, L. Gardner, Proposed overstrength for AISC 370 and ASCE 8, SCI Report, 2020.

[70] X. Meng, L. Gardner, Behavior and Design of Normal- and High-Strength Steel SHS and RHS Columns, J. Struct. Eng. 146 (2020) 04020227.

[71] X. Meng, L. Gardner, A.J. Sadowski, J.M. Rotter, Elasto-plastic behaviour and design of semi-compact circular hollow sections, Thin-Walled Struct. 148 (2020) 106486.

[72] SAFEBRICTILE. 2016. Standardization of safety assessment procedures across brittle to ductile failure modes. Grant Agreement Number: RFSR-CT-2013-00023, Deliverable D1.1 - Guideline for the Safety Assessment of Design Rules for Steel Structures in Line with EN 1990.

[73] HOLLOSSTAB. 2019. Overall-slenderness based direct design for strength and stability of innovative hollow sections. Grant Agreement Number: RFCS-2015-709892, Deliverable D7.2 - Reliability Analysis of the Design Proposals and Determination of Partial Factors.

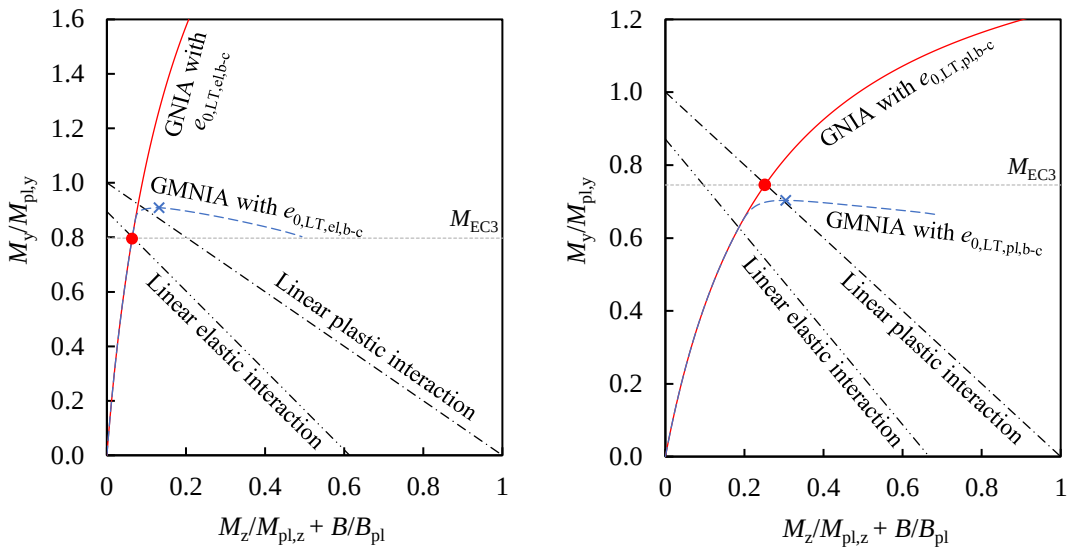


(a) HEA 160 (Class 3), S355, $\bar{\lambda}_{LT}$ = 0.6 (b) HEA 1000 (Class 2), S420, $\bar{\lambda}_{LT}$ = 0.8

Fig. 1 Normalised second-order internal moments at the critical cross-section and linear cross-section interaction curves for members subjected to uniform major axis bending, obtained from GNIA and GMNIA using the back-calculated (a) elastic $e_{0,LT,el,b\text{-}c}$ and (b) plastic $e_{0,LT,pl,b\text{-}c}$ equivalent imperfections compared against the prEN 1993-1-1 member buckling resistance $M_{EC3}$

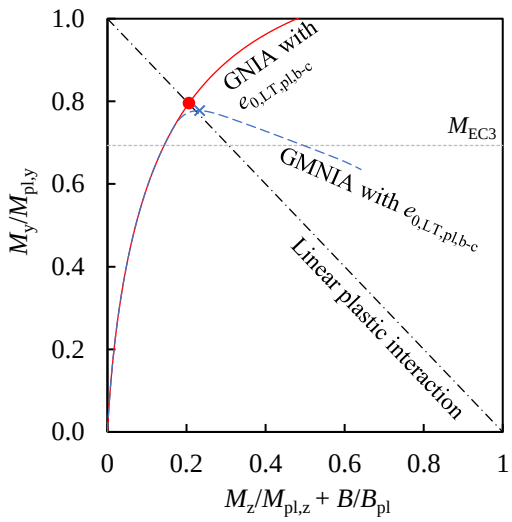


Fig. 2 Normalised second-order internal moments at the critical cross-section and linear plastic cross-section interaction curve for a hot-rolled S420 steel HEA 100 (Class 1) member with $\bar{\lambda}_{LT}$ = 1.0 subjected to uniform major axis bending, obtained from GNIA and GMNIA using the back-calculated plastic equivalent imperfection $e_{0,LT,pl,b\text{-}c}$ compared against the prEN 1993-1-1 member buckling resistance $M_{EC3}$

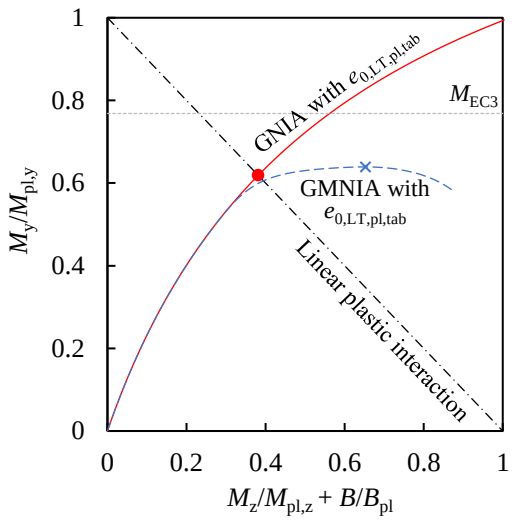


Fig. 3 Normalised second-order internal moments at the critical cross-section and linear plastic cross-section interaction curve for a hot-rolled S420 steel IPE 140 (Class 1) member with $\bar{\lambda}_{LT}$ = 0.8 subjected to uniform major axis bending, obtained from GNIA and GMNIA using the tabulated plastic equivalent imperfection $e_{0,LT,pl,tab}$ compared against the prEN 1993-1-1 member buckling resistance $M_{EC3}$

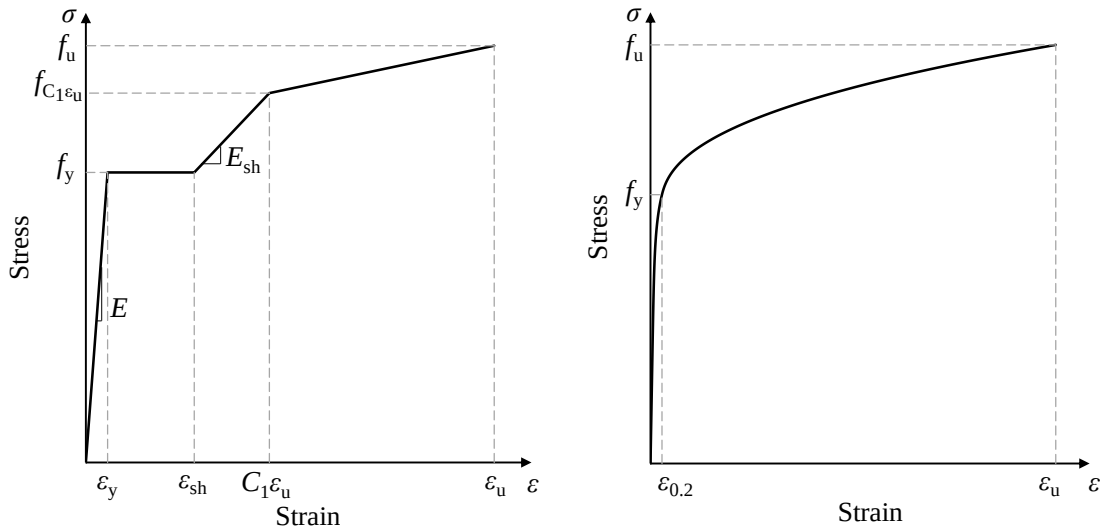


(a) Quad-linear material model for hot-rolled steel [36]

(b) Two-stage Ramberg-Osgood material model for stainless steel [39]

Fig. 4 Material stress-strain models adopted for (a) hot-rolled steel and (b) stainless steel

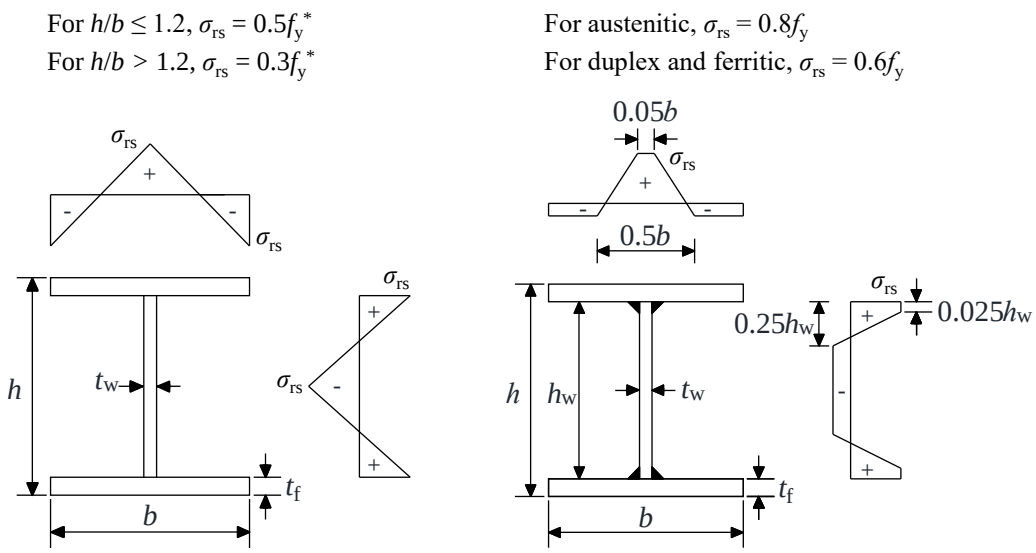


(a) ECCS [20] model for hot-rolled steel I-sections ($f_y^*$ = 235 MPa)

(b) Yuan et al. [44] model for welded stainless steel I-sections

Fig. 5 Residual stress patterns adopted for (a) hot-rolled steel and (b) welded stainless steel I-sections (+ve = tension; -ve = compression)

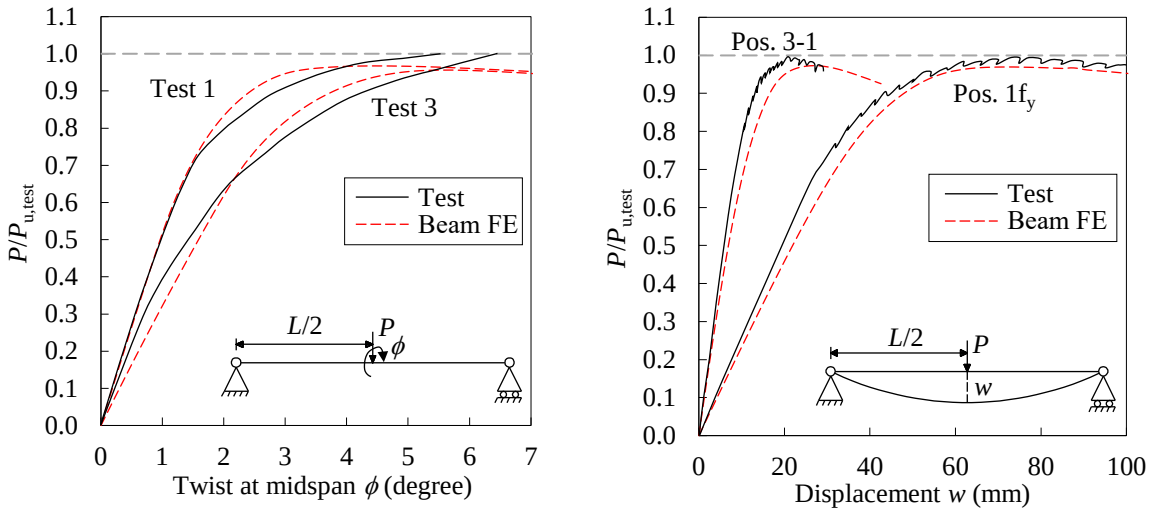


(a) Specimens Test 1 and Test 3 tested in [62,63]

(b) Specimens Pos. 3-1 and Pos. 1$f_y$ tested in [64]

Fig. 6 Comparison of experimental and numerical load-deformation curves of members subjected to 3-point bending with eccentrically applied vertical loading at midspan, tested in [62,63] and [64]

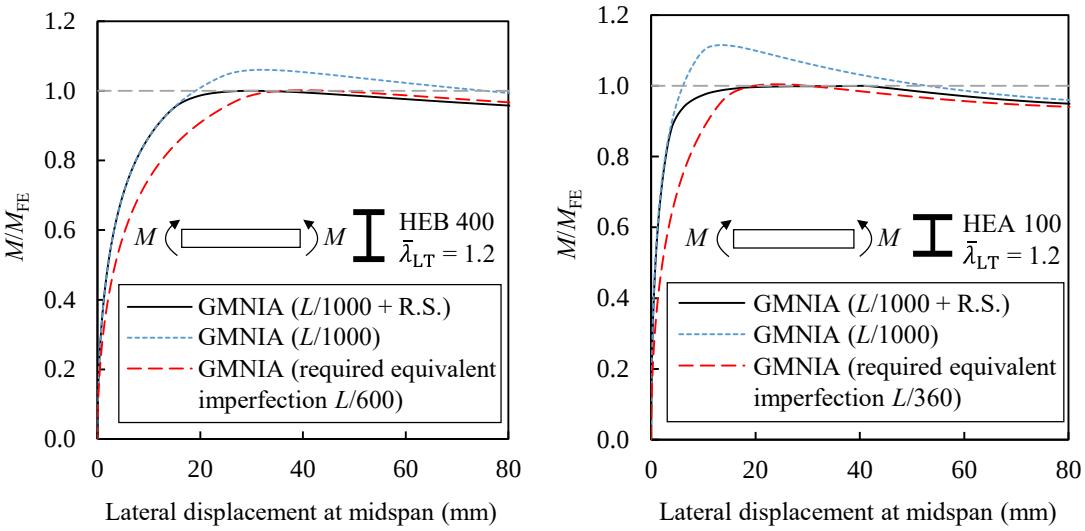


(a) Hot-rolled HEB 400 ($h/b > 1.2$)

(b) Hot-rolled HEB 100 ($h/b \leq 1.2$)

Fig. 7 Required equivalent imperfections $e_{0,\mathrm{req}}$ calculated iteratively to obtain ultimate bending moment $M_{\mathrm{u}}$ within 0.5% of the benchmark ultimate bending moments $M_{\mathrm{FE}}$ obtained from GMNIA of members with geometric imperfection magnitudes of $L/1000$ and residual stresses (R.S.)

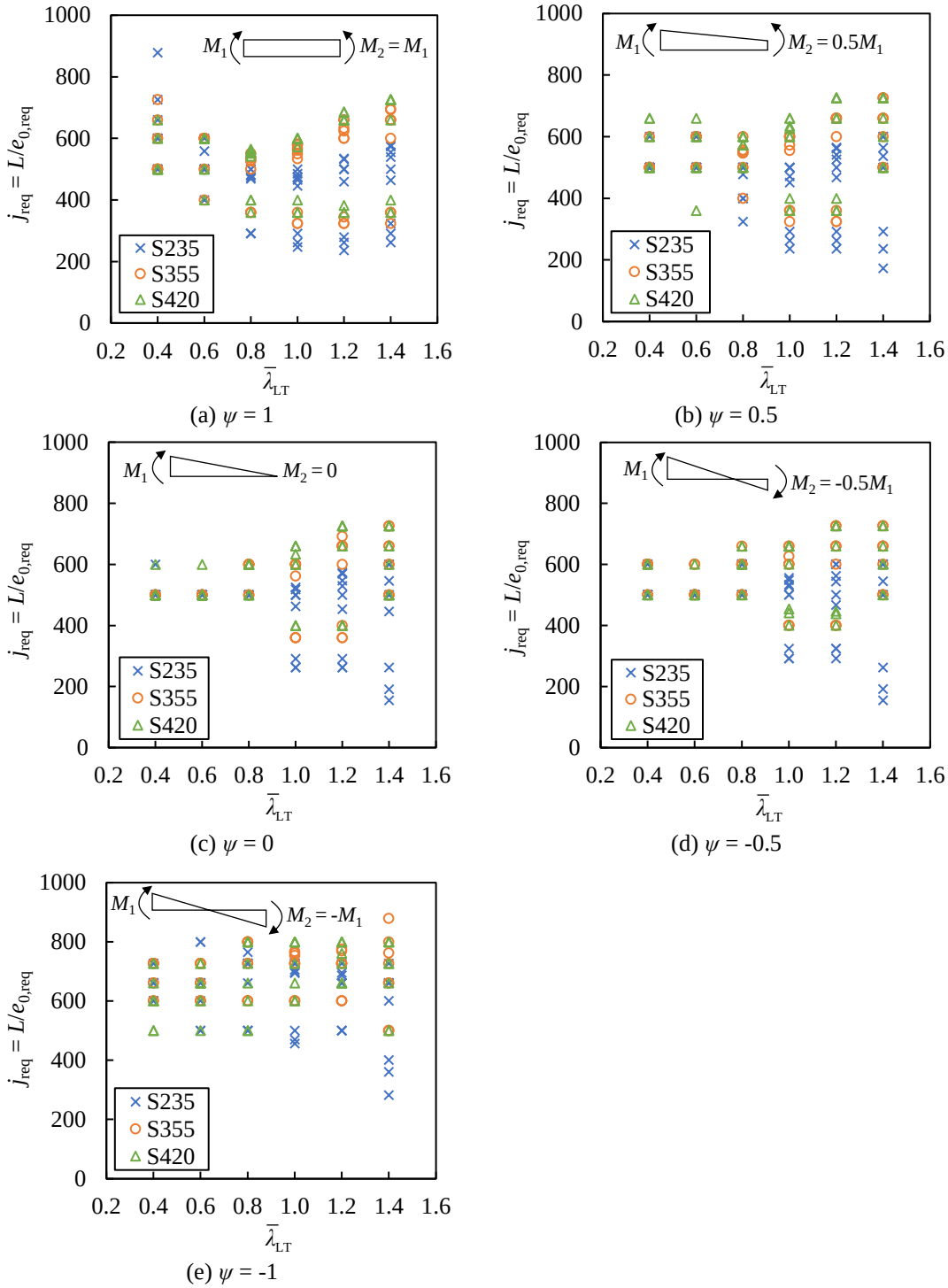


Fig. 8 Required values of non-dimensional equivalent imperfections $j_{req} = L/e_{0,req}$ for hot-rolled steel members subjected to different bending moment distributions along the member length ($\psi$ = 1, 0.5, 0, -0.5 and -1), achieved by changing the ratio of the applied end moments $\psi = M_2/M_1$

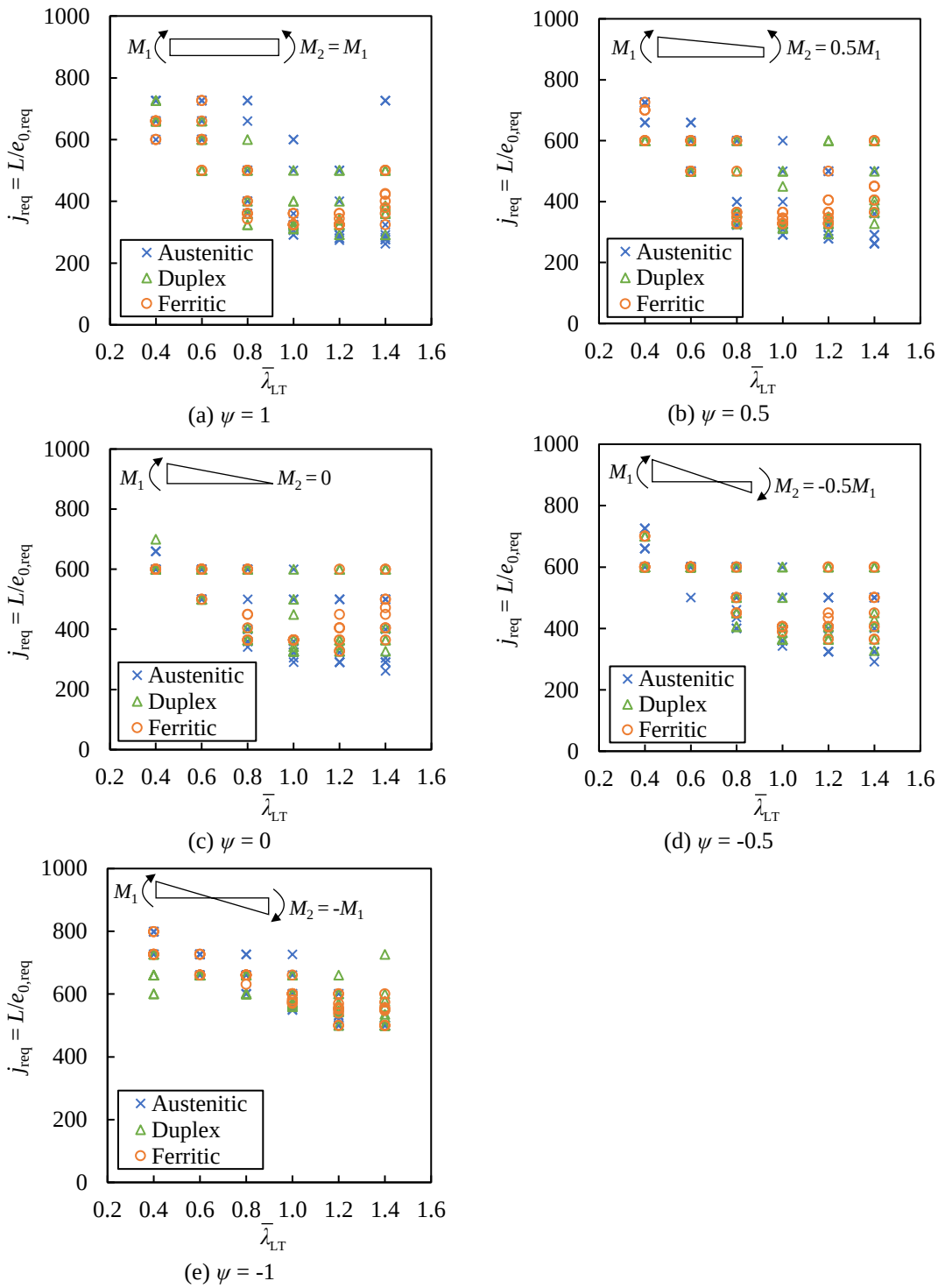


Fig. 9 Required values of $j_{req} = L/e_{0,req}$ for stainless steel members subjected to different bending moment distributions along the member length ($\psi$ = 1, 0.5, 0, -0.5 and -1), achieved by changing the ratio of the applied end moments $\psi = M_2/M_1$

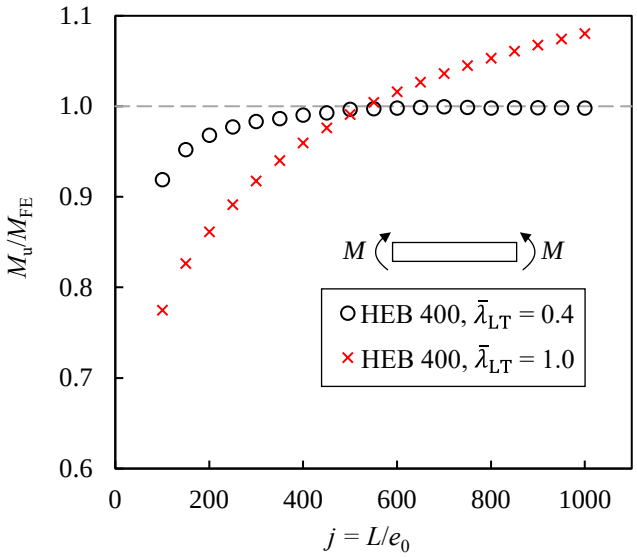


Fig. 10 Sensitivity to geometric imperfections of hot-rolled S355 steel HEB 400 members with LTB slenderness $\bar{\lambda}_{LT}$ = 0.4 and 1.0 subjected to uniform bending

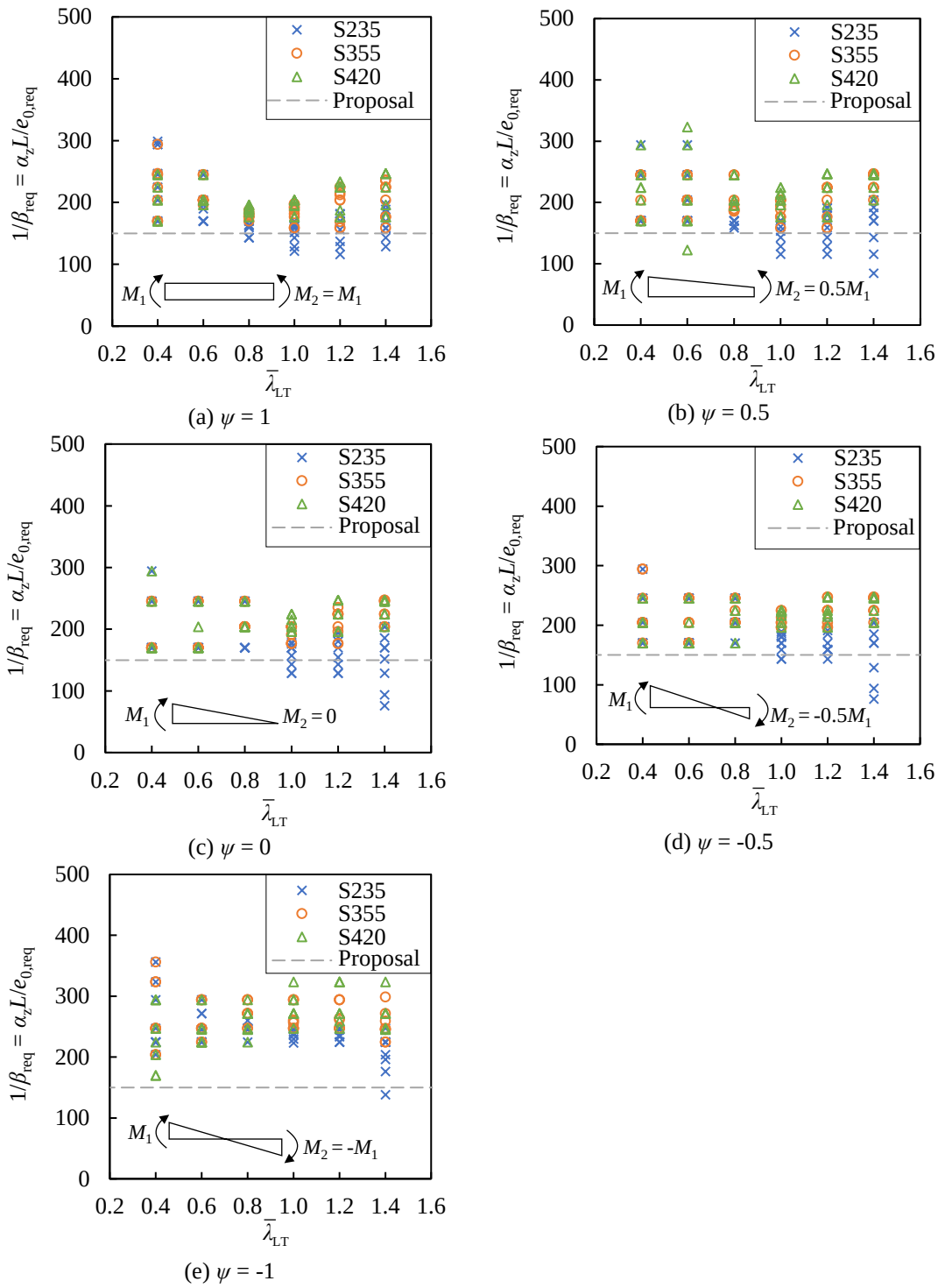


Fig. 11 Required values of $1/\beta_{req}$ for hot-rolled steel members subjected to different bending moment distributions along the member length ($\psi$ = 1, 0.5, 0, -0.5 and -1), achieved by changing the ratio of the applied end moments $\psi = M_2/M_1$

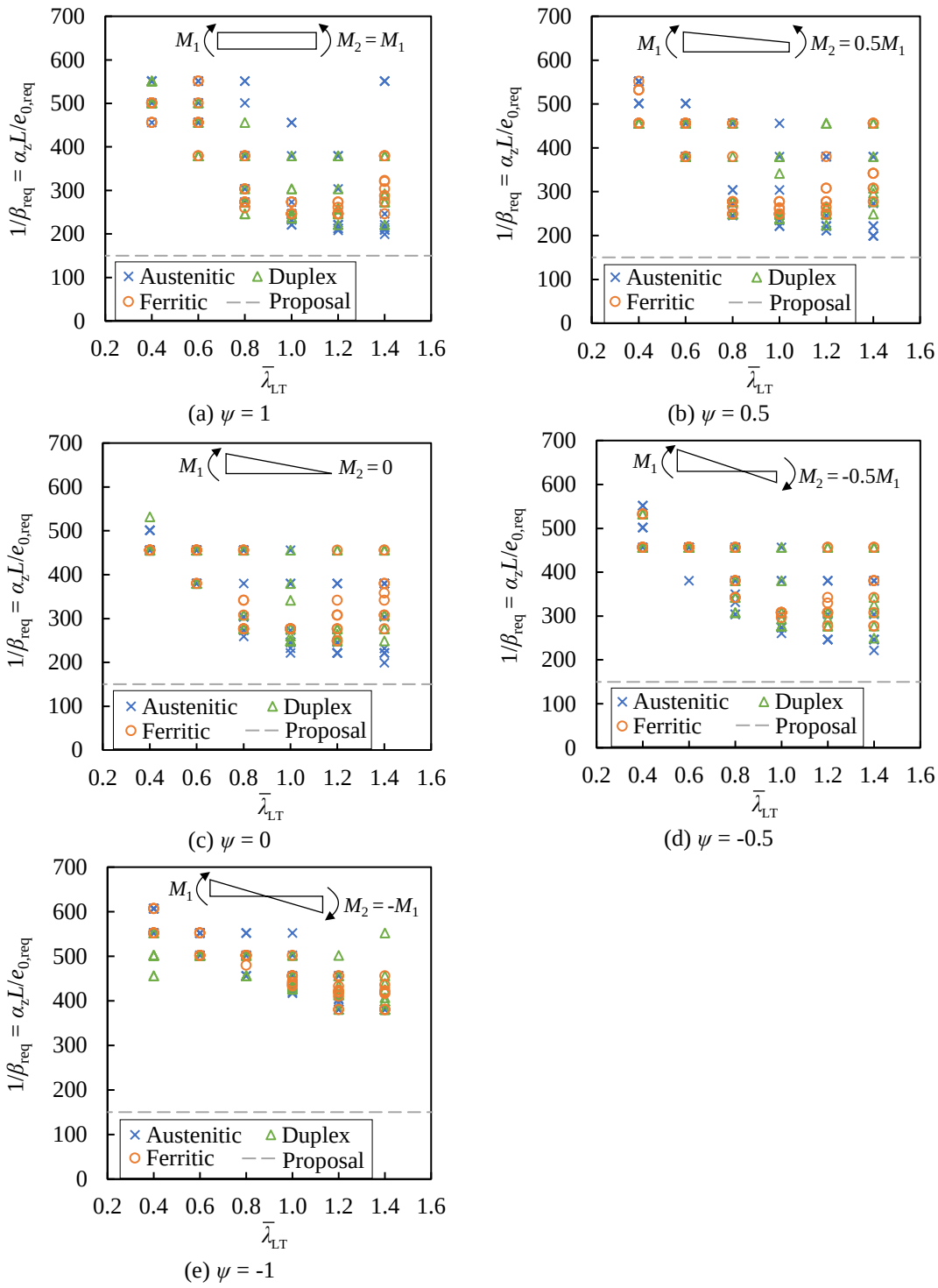


Fig. 12 Required values of $1/\beta_{req}$ for stainless steel members subjected to different bending moment distributions along the member length ($\psi$ = 1, 0.5, 0, -0.5 and -1), achieved by changing the ratio of the applied end moments $\psi = M_2/M_1$

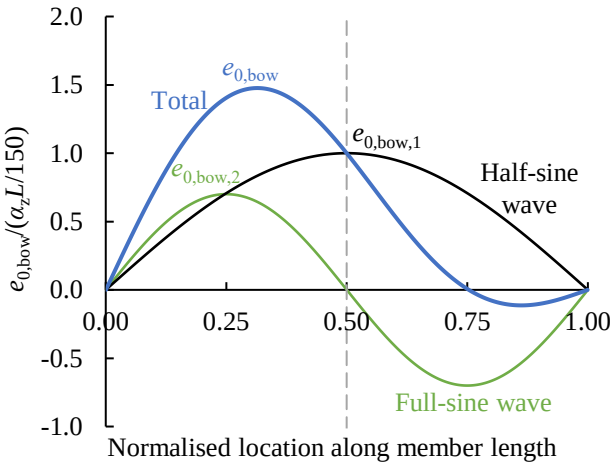


Fig. 13 Direct modelling of lateral bow equivalent imperfection $e_{0,bow}$ through summation of a half-sine wave with amplitude $e_{0,bow,1} = \alpha_z L/150$ and a full-sine wave with amplitude $e_{0,bow,2} = \alpha_z L/215$

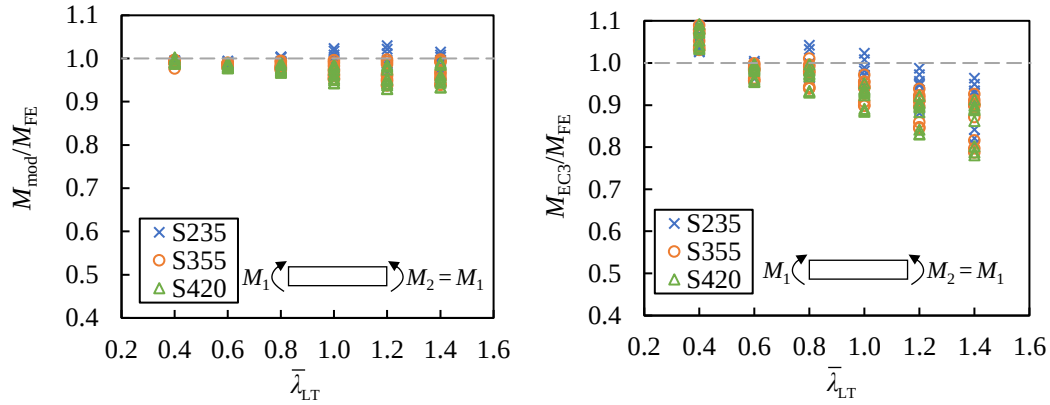


(a) $\psi$ = 1

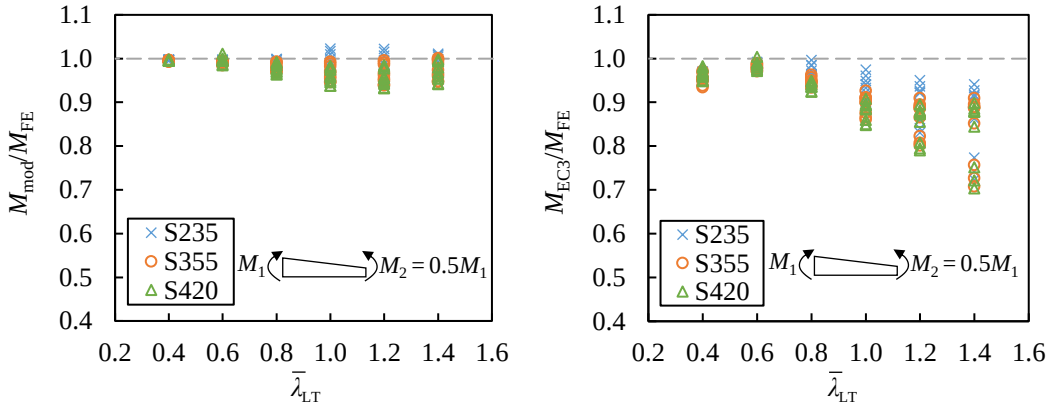


(b) $\psi$ = 0.5

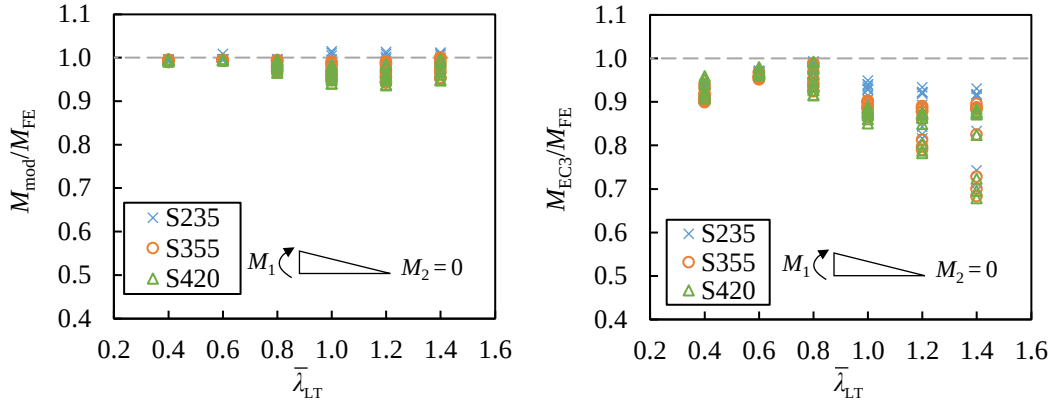


(c) $\psi$ = 0

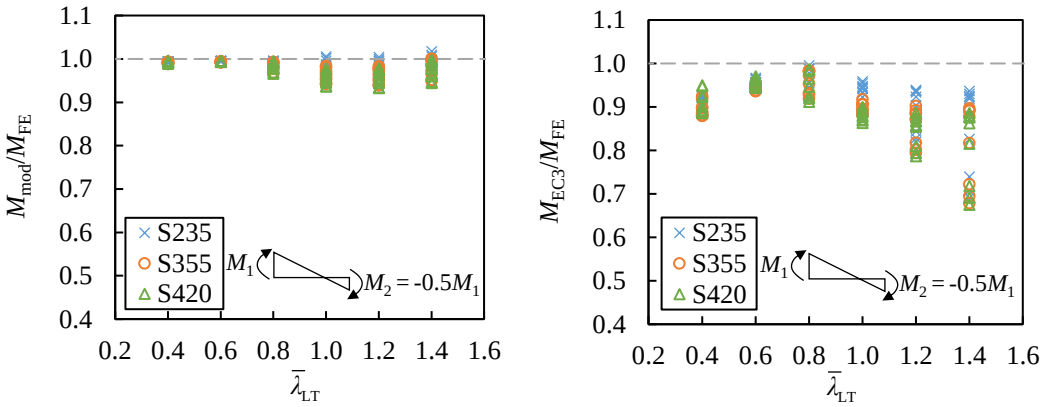


(d) $\psi$ = -0.5

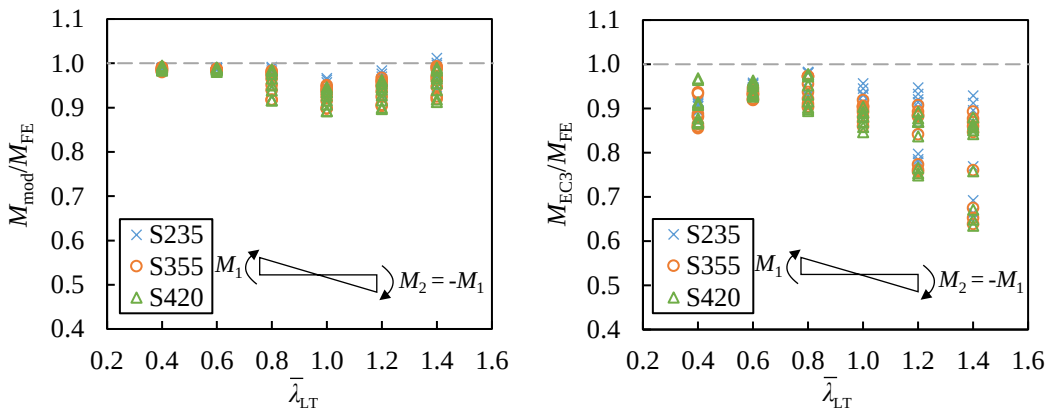


(e) $\psi$ = -1

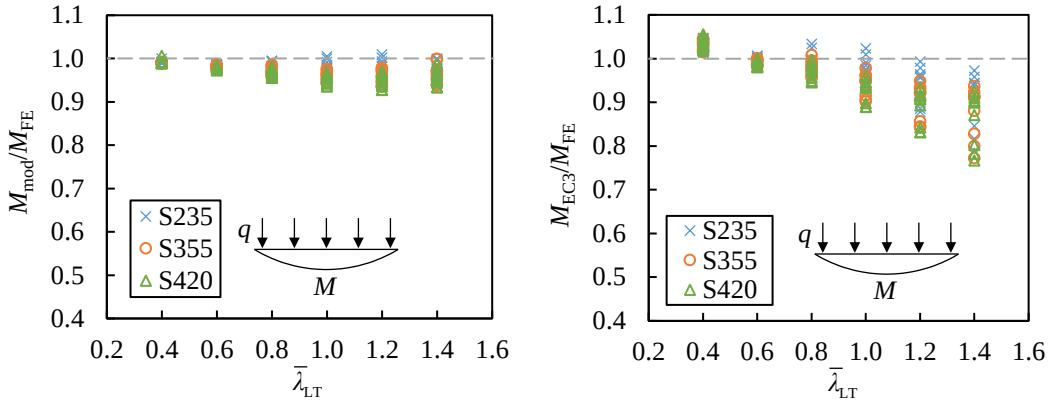


(f) Uniformly distributed load

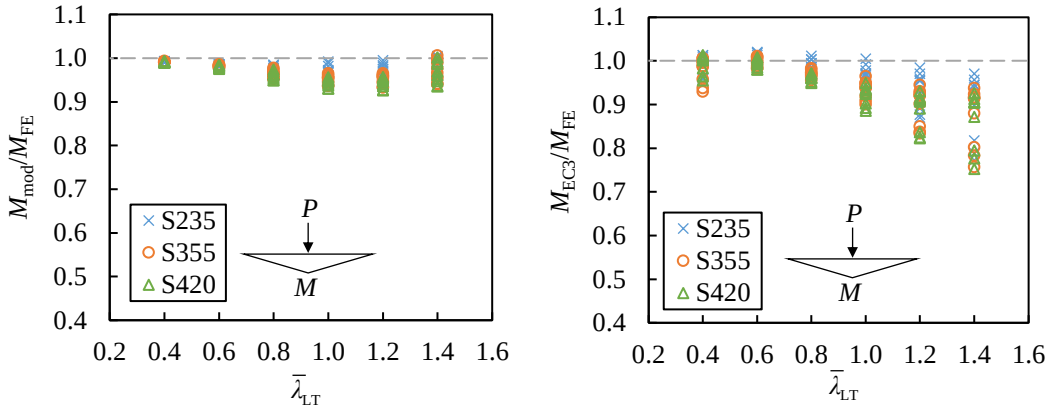


(g) Point load

Fig. 14 Comparisons of the ultimate resistance predictions obtained using the proposed equivalent imperfections based on the first LTB eigenmode $M_{mod}$ and using the prEN 1993-1-1 LTB curves $M_{EC3}$, with the benchmark results $M_{FE}$, for hot-rolled steel members subjected to different loading conditions

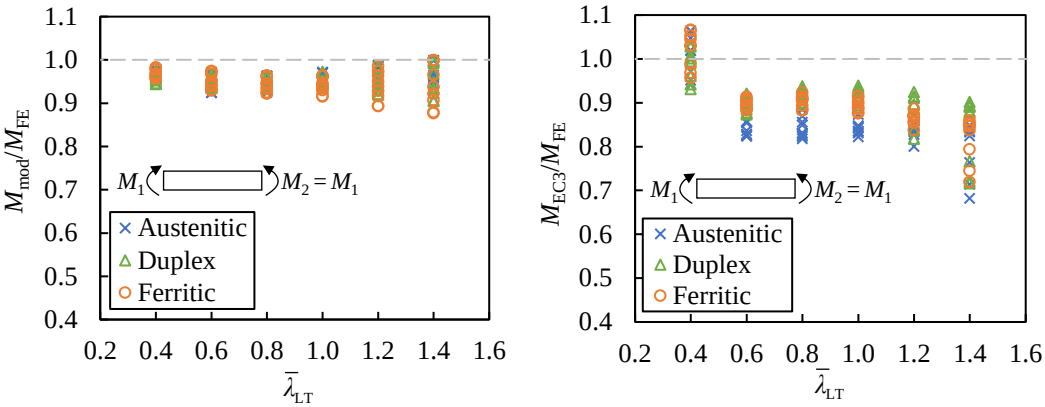


(a) $\psi$ = 1

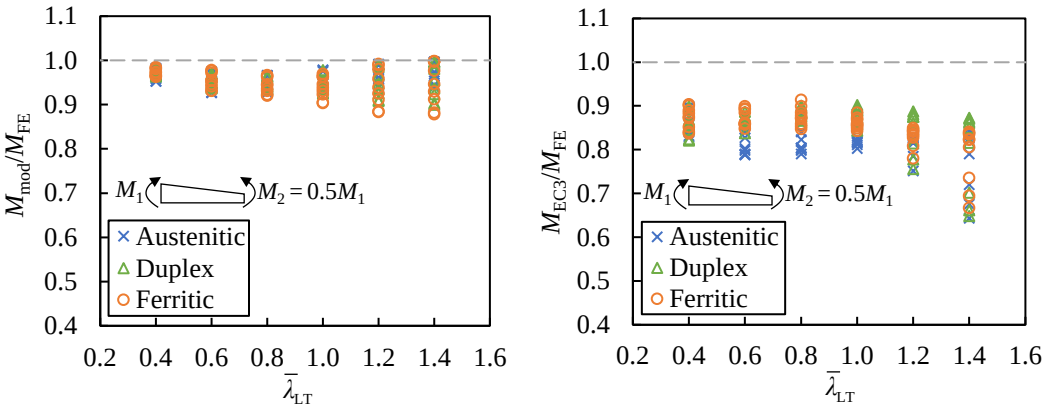


(b) $\psi$ = 0.5

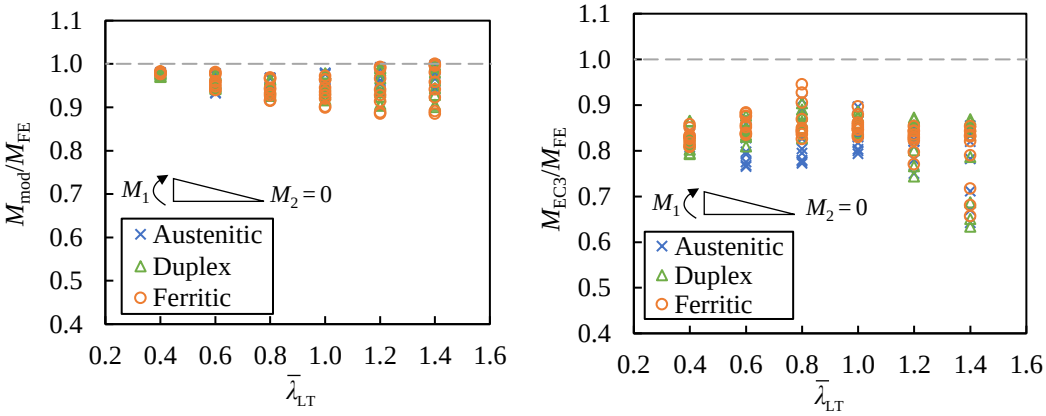


(c) $\psi$ = 0

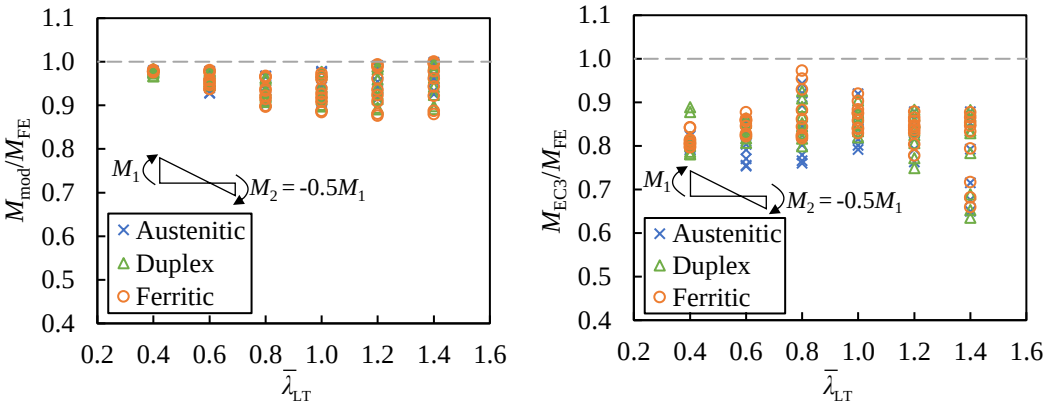


(d) $\psi$ = -0.5

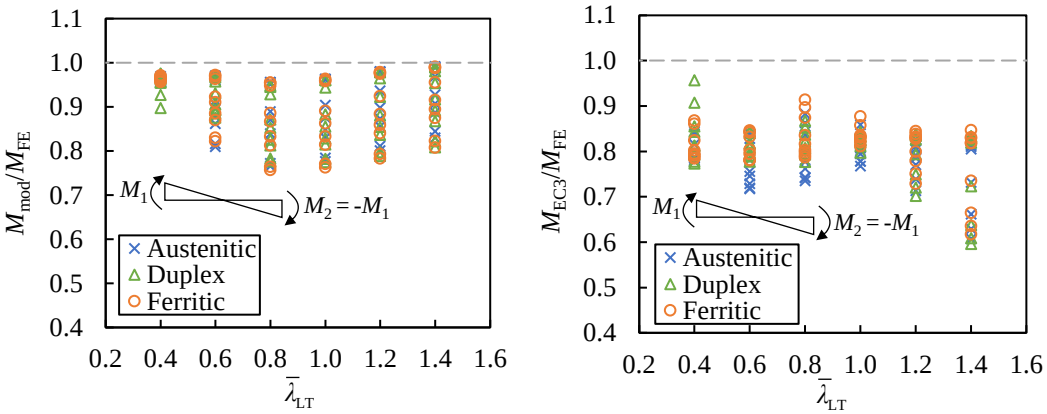


(e) $\psi$ = -1

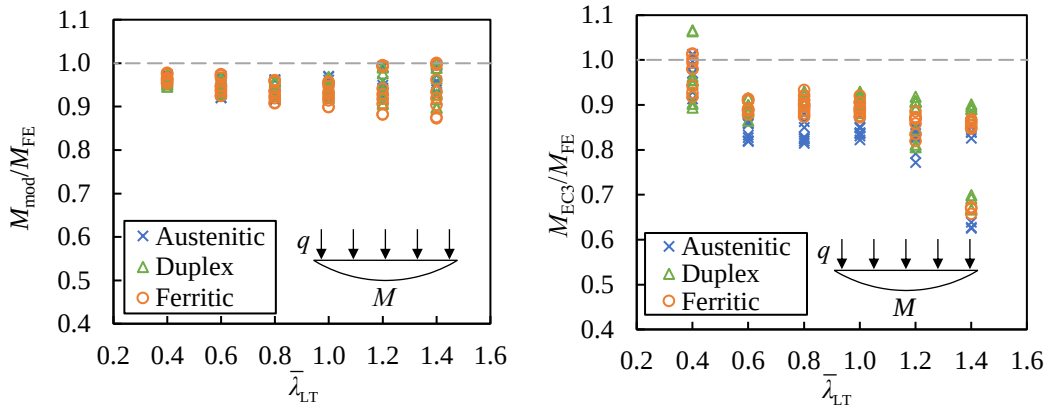


(f) Uniformly distributed load

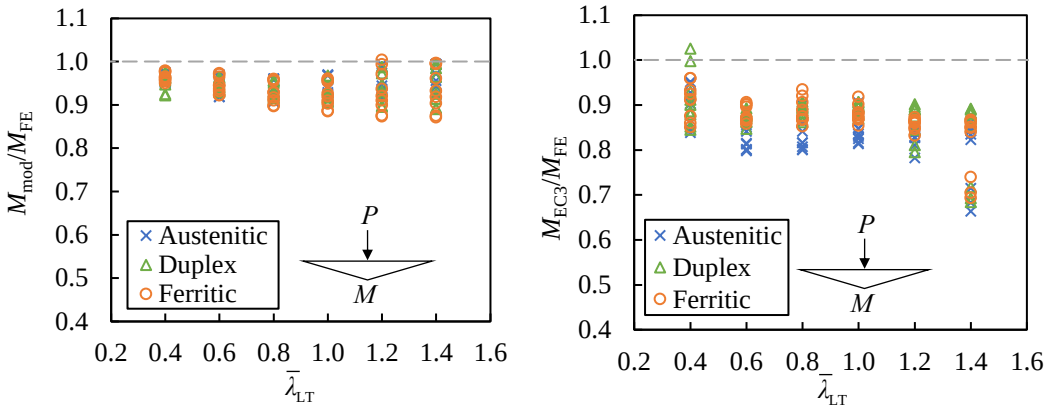


(g) Point load

Fig. 15 Comparisons of the ultimate resistance predictions obtained using the proposed equivalent imperfections based on the first LTB eigenmode $M_{mod}$ and using the prEN 1993-1-4 LTB curves $M_{EC3}$, with the benchmark results $M_{FE}$, for stainless steel members subjected to different loading conditions

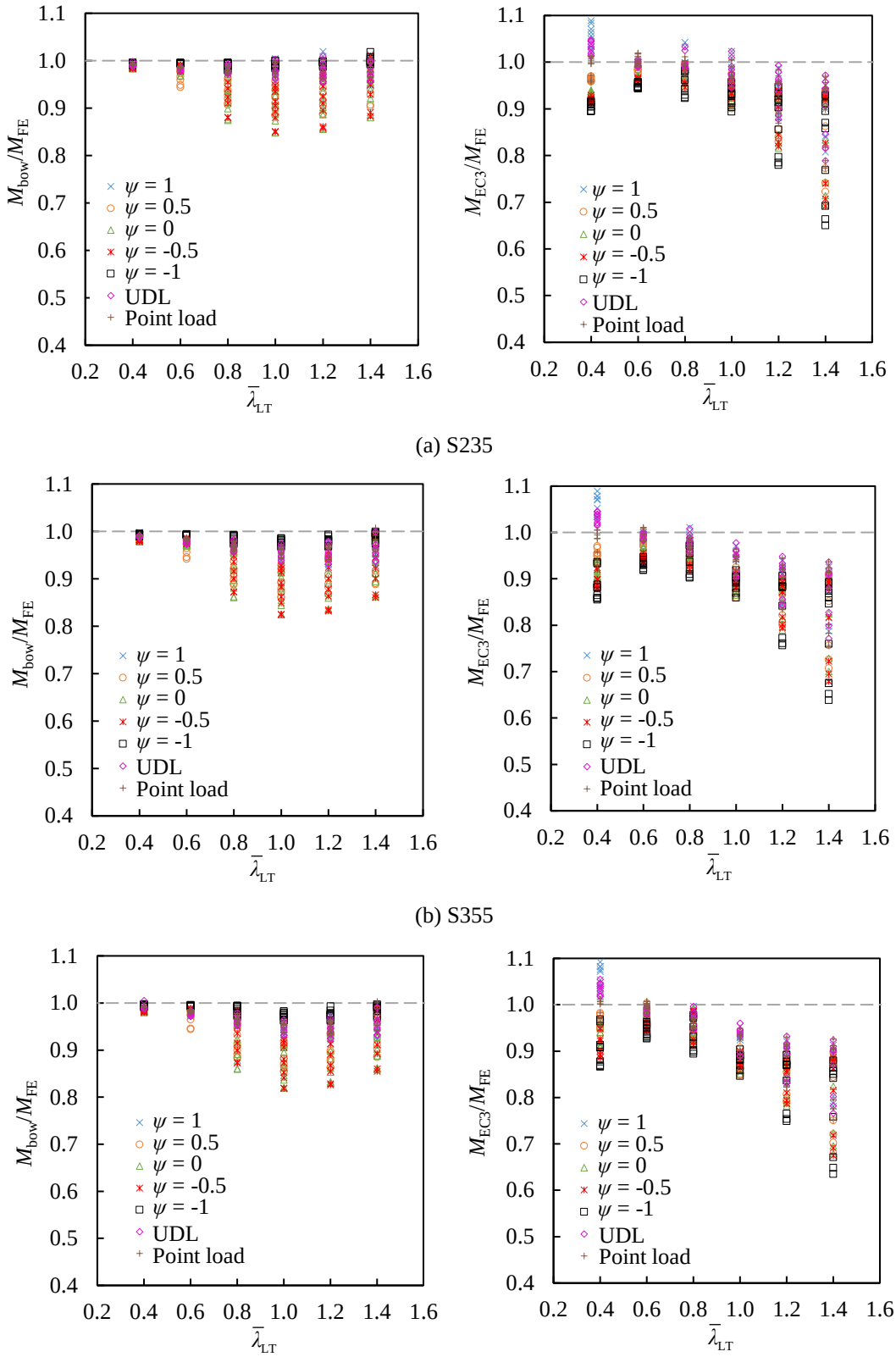


(a) S235

(b) S355

(c) S420

Fig. 16 Comparisons of the ultimate resistance predictions obtained using the proposed equivalent imperfections based on the combined half and full sine wave lateral bow shapes $M_{bow}$ and using the prEN 1993-1-1 LTB curves $M_{EC3}$, with the benchmark results $M_{FE}$, for hot-rolled steel members subjected to different loading conditions

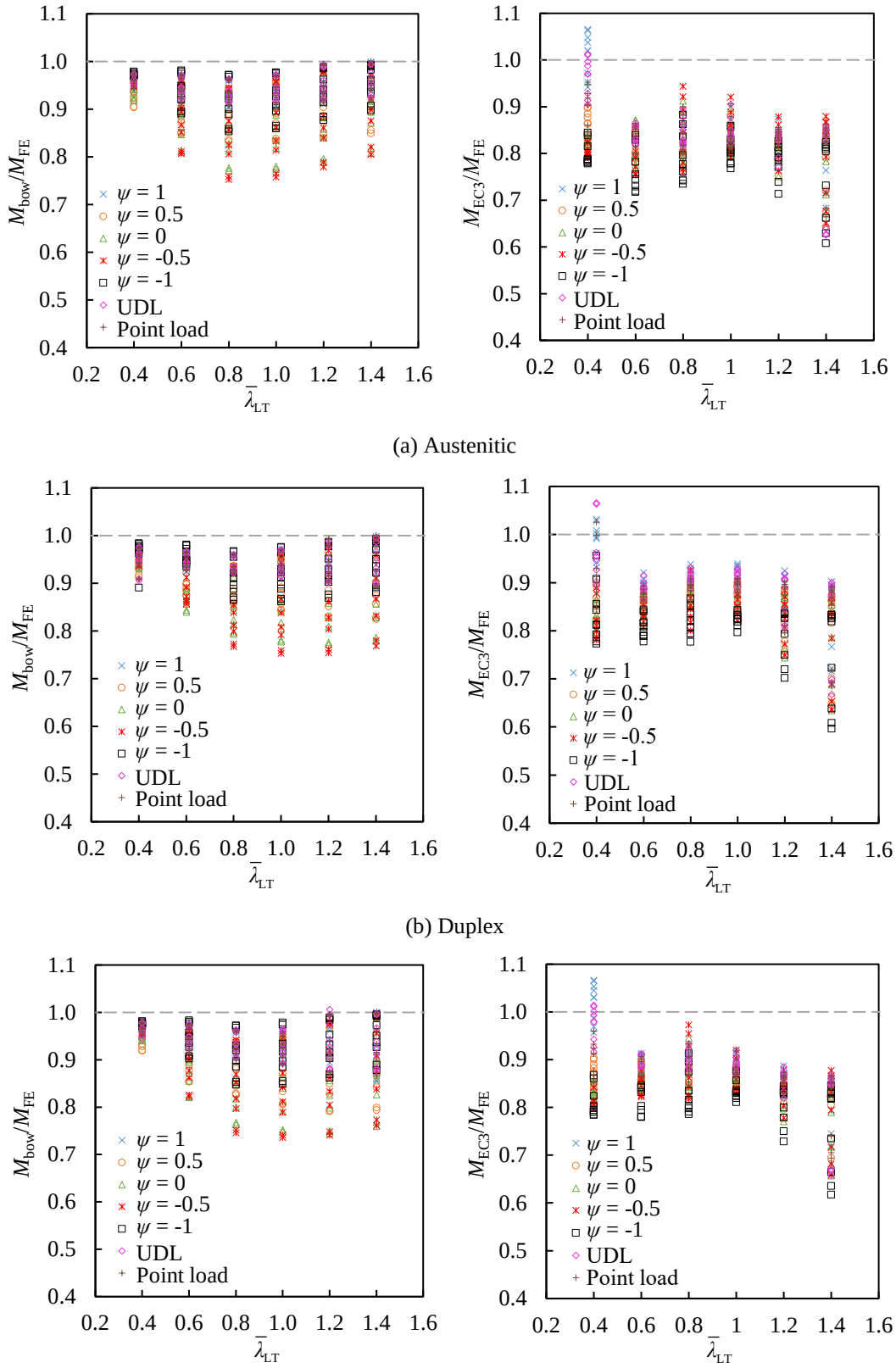


(a) Austenitic

(b) Duplex

(c) Ferritic

Fig. 17 Comparisons of the ultimate resistance predictions obtained using the proposed equivalent imperfections based on the combined half and full sine wave lateral bow shapes $M_{bow}$ and using the prEN 1993-1-4 LTB curves $M_{EC3}$, with the benchmark results $M_{FE}$, for stainless steel members subjected to different loading conditions

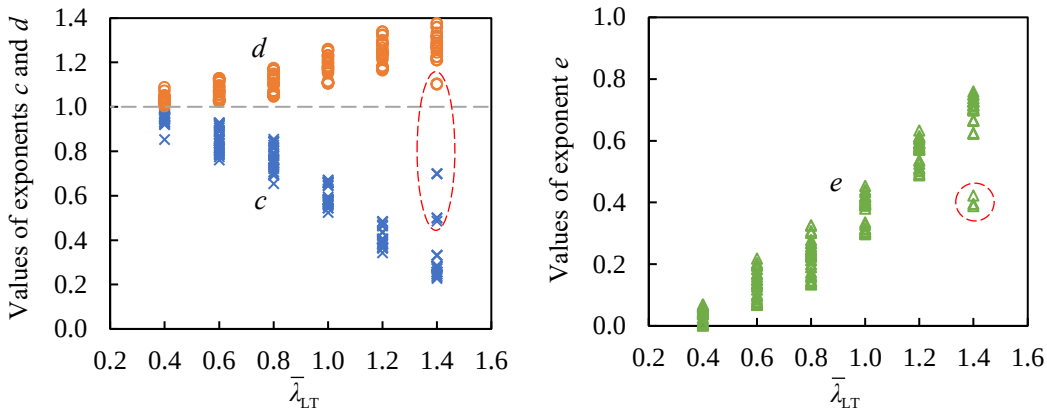


(a) Hot-rolled steel members with $e_{0,mod}$, as defined in Table 6

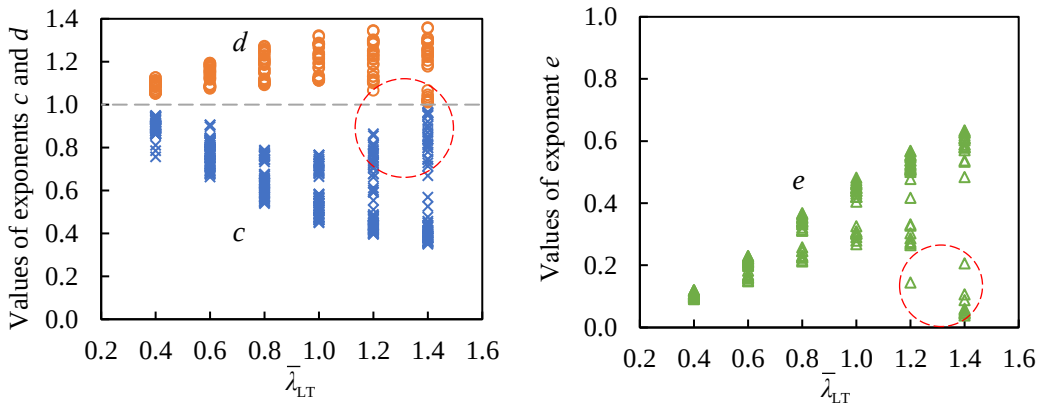


(b) Stainless steel members with $e_{0,bow}$, as defined in Table 6

Fig. 18 Values of exponents *c*, *d* and *e* reflecting the dependency of the ultimate member resistances on the yield stress $f_y$, plastic major axis section modulus $W_{pl,y}$ and Young's modulus *E*, respectively, obtained through the design method (a) using the proposed imperfections $e_{0,mod}$ defined using the LTB eigenmode for the considered hot-rolled steel members and (b) using the proposed lateral imperfections $e_{0,bow}$ for the considered stainless steel members, subjected to uniform bending.

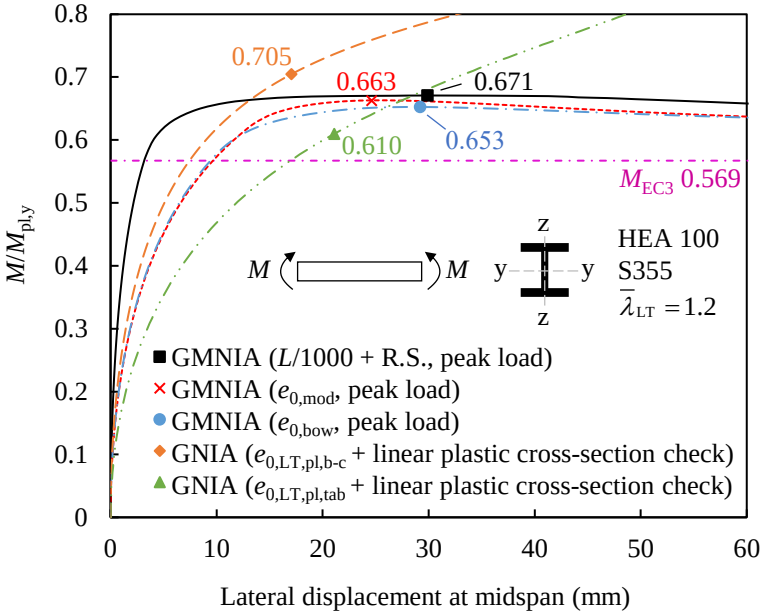


(a) Worked example 1: HEA 100, S355, $\bar{\lambda}_{LT}$ = 1.2

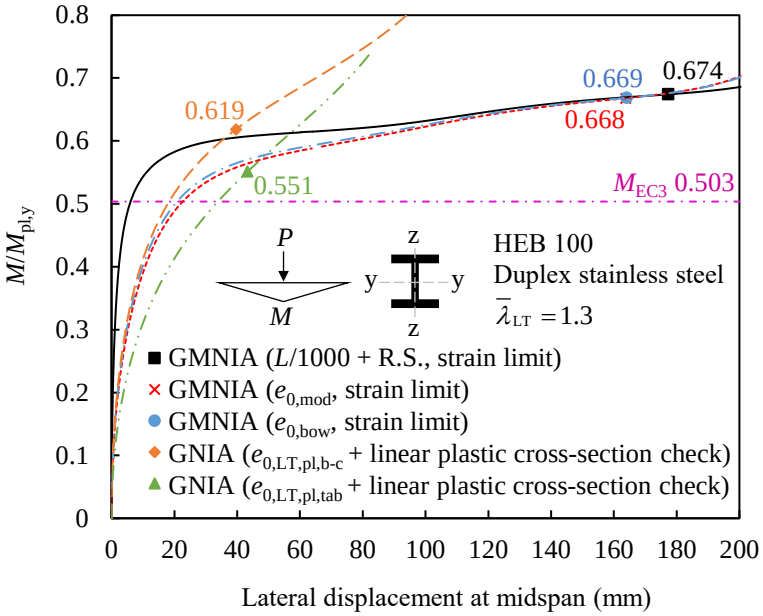


(b) Worked example 2: HEB 100, duplex stainless steel, $\bar{\lambda}_{LT}$ = 1.3

Fig. 19 Load-deformation paths and ultimate member resistance predictions for worked examples obtained from different design approaches

**Table 1** Imperfection factor $\alpha_{LT}$ for lateral-torsional buckling of doubly symmetric I- and H-sections [12, 14]

| Material | Grade | Limits | | $\alpha_{LT}$ |
|---|---|---|---|---|
| Hot-rolled steel | - | $h/b > 1.2$ | $t_f \leq 40$ mm | $0.12\sqrt{W_{el,y}/W_{el,z}} \leq 0.34$ |
| | | | $t_f > 40$ mm | $0.16\sqrt{W_{el,y}/W_{el,z}} \leq 0.49$ |
| | | $h/b \leq 1.2$ | - | $0.16\sqrt{W_{el,y}/W_{el,z}} \leq 0.49$ |
| Stainless steel | Austenitic | - | | $0.37\sqrt{W_{el,y}/W_{el,z}} \leq 1.10$ |
| | Duplex | | | $0.23\sqrt{W_{el,y}/W_{el,z}} \leq 0.76$ |
| | Ferritic | | | $0.27\sqrt{W_{el,y}/W_{el,z}} \leq 0.76$ |

**Table 2** Reference relative bow imperfection $\beta_{LT}$ for use in lateral-torsional buckling design by second-order elastic analysis [12]

| Cross-section | Condition | Elastic cross-section verification | Plastic cross-section verification |
|---|---|---|---|
| Rolled | $h/b \leq 2.0$ | 1/250 | 1/200 |
| | $h/b > 2.0$ | 1/200 | 1/150 |
| Welded | $h/b \leq 2.0$ | 1/200 | 1/150 |
| | $h/b > 2.0$ | 1/150 | 1/100 |

**Table 3** Overview of adopted material parameters for the FE models [1, 36, 38]

| Material | Grade | Young's modulus $E$ (N/mm$^2$) | Yield (0.2% proof) stress $f_y$ (N/mm$^2$) | Ultimate stress $f_u$ (N/mm$^2$) | Strain hardening strain $\varepsilon_{sh}$ | Ultimate strain $\varepsilon_u$ | Strain hardening exponent $n$ | Strain hardening exponent $m$ |
|---|---|---|---|---|---|---|---|---|
| Hot-rolled Steel | S235 | 210000 | 235 | 360 | 0.015 | 0.21 | - | - |
| | S355 | | 355 | 510 | 0.015 | 0.18 | | |
| | S420 | | 420 | 520 | 0.026 | 0.12 | | |
| Stainless steel | A | 200000 | 280 | 580 | - | 0.50 | 9.1 | 2.3 |
| | D | | 530 | 770 | | 0.30 | 9.3 | 3.6 |
| | F | | 320 | 480 | | 0.16 | 17.2 | 2.8 |

**Table 4** Summary of validation study for beam finite element models against experimental results from literature

| Reference | Load configuration | No. of tests | $\alpha_{u,FE}/\alpha_{u,test}$ | |
|---|---|---|---|---|
| | | | Mean | CoV |
| Dux & Kitipornchai (1983) [60] | 3-point bending; 4-point bending | 9 | 0.969 | 0.015 |
| Lindner & Glitsch (2004) [61] | 3-point bending with eccentricity | 13 | 0.951 | 0.028 |
| Tusnin & Prokic (2015) [62, 63] | 3-point bending with eccentricity | 6 | 0.898 | 0.055 |
| Schaper et al. (2019) [64] | 3-point bending with eccentricity | 7 | 1.006 | 0.036 |
| Demirhan et al. (2020) [65] | Cantilever beams | 9 | 1.009 | 0.140 |
| Total | | 44 | 0.968 | 0.081 |

**Table 5** Imperfection factor $\alpha_z$ for flexural buckling of doubly symmetric I- and H-sections [12, 14]

| Material | Limits | | $\alpha_z$ |
|---|---|---|---|
| Hot-rolled steel | $h/b > 1.2$ | $t_f \leq 40$ mm | 0.34 |
| | | $t_f > 40$ mm | 0.49 |
| | $h/b \leq 1.2$ | | 0.49 |
| Stainless steel | - | | 0.76 |

**Table 6** Proposed equivalent geometric imperfections for out-of-plane stability design of steel and stainless steel members by GMNIA

| Imperfection | Shape | $\beta_{LT}$ | Illustration |
|---|---|---|---|
| $e_{0,mod}$ | LTB eigenmode* | $\beta_{LT} = 1/150$ | 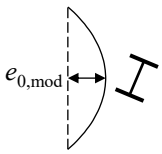  |
| $e_{0,bow}$ | Lateral bow | $\beta_{LT,1} = 1/150$ (half-sine wave) + $\beta_{LT,2} = 1/215$ (full-sine wave) | 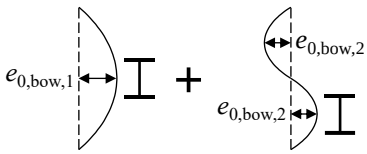  |

*Eigenmode can be with or without twist with minimal effect on results.

**Table 7** Summary of mean values of member resistance predictions obtained using design methods with LTB eigenmode equivalent imperfections $M_{mod}$, lateral bow equivalent imperfections $M_{bow}$ and prEN 1993-1-1 LTB curves $M_{EC3}$, normalised by benchmark FE results $M_{FE}$, for all considered cases

| Load case | No. | Hot-rolled steel | | | Stainless steel | | |
|---|---|---|---|---|---|---|---|
| | | $M_{mod}/M_{FE}$ | $M_{bow}/M_{FE}$ | $M_{EC3}/M_{FE}$ | $M_{mod}/M_{FE}$ | $M_{bow}/M_{FE}$ | $M_{EC3}/M_{FE}$ |
| $\psi$ = 1 | 162 | 0.980 | 0.968 | 0.957 | 0.952 | 0.943 | 0.890 |
| $\psi$ = 0.5 | 162 | 0.982 | 0.938 | 0.918 | 0.954 | 0.905 | 0.841 |
| $\psi$ = 0 | 162 | 0.984 | 0.932 | 0.906 | 0.957 | 0.888 | 0.828 |
| $\psi$ = -0.5 | 162 | 0.982 | 0.938 | 0.904 | 0.951 | 0.891 | 0.830 |
| $\psi$ = -1 | 162 | 0.962 | 0.989 | 0.886 | 0.902 | 0.940 | 0.798 |
| UDL | 162 | 0.973 | 0.971 | 0.958 | 0.947 | 0.944 | 0.877 |
| Point load | 162 | 0.970 | 0.975 | 0.947 | 0.943 | 0.946 | 0.862 |

**Table 8** Summary of the reliability analysis results for the proposed approach applied to hot-rolled steel members subjected to different loading conditions assessed against benchmark FE results

| Load case | Grade | No. | $f_{y,mean}/f_{y,nom}$ | $V_{fy}$ | $V_{Wpl,y}$ | $V_E$ | Mode imperfection $e_{0,mod}$ | | | Lateral imperfection $e_{0,bow}$ | | |
|---|---|---|---|---|---|---|---|---|---|---|---|---|
| | | | | | | | $b$ | $V_\delta$ | $\gamma_{M1}^*$ | $b$ | $V_\delta$ | $\gamma_{M1}^*$ |
| $\psi$ = 1 | S235 | 54 | 1.25 | 0.055 | 0.029 | 0.03 | 1.008 | 0.014 | 1.013 | 1.020 | 0.017 | 1.005 |
| | S355 | 54 | 1.20 | 0.050 | 0.029 | 0.03 | 1.025 | 0.018 | 1.024 | 1.037 | 0.024 | 1.018 |
| | S420 | 54 | 1.20 | 0.050 | 0.029 | 0.03 | 1.030 | 0.021 | 1.021 | 1.043 | 0.026 | 1.016 |
| $\psi$ = 0.5 | S235 | 54 | 1.25 | 0.055 | 0.029 | 0.03 | 1.007 | 0.013 | 1.016 | 1.055 | 0.036 | 1.004 |
| | S355 | 54 | 1.20 | 0.050 | 0.029 | 0.03 | 1.022 | 0.019 | 1.028 | 1.073 | 0.045 | 1.028 |
| | S420 | 54 | 1.20 | 0.050 | 0.029 | 0.03 | 1.026 | 0.022 | 1.029 | 1.076 | 0.049 | 1.034 |
| $\psi$ = 0 | S235 | 54 | 1.25 | 0.055 | 0.029 | 0.03 | 1.007 | 0.012 | 1.013 | 1.064 | 0.050 | 1.025 |
| | S355 | 54 | 1.20 | 0.050 | 0.029 | 0.03 | 1.020 | 0.017 | 1.028 | 1.081 | 0.059 | 1.056 |
| | S420 | 54 | 1.20 | 0.050 | 0.029 | 0.03 | 1.023 | 0.020 | 1.029 | 1.084 | 0.063 | 1.058 |
| $\psi$ = -0.5 | S235 | 54 | 1.25 | 0.055 | 0.029 | 0.03 | 1.011 | 0.012 | 1.009 | 1.057 | 0.049 | 1.029 |
| | S355 | 54 | 1.20 | 0.050 | 0.029 | 0.03 | 1.022 | 0.018 | 1.025 | 1.074 | 0.058 | 1.057 |
| | S420 | 54 | 1.20 | 0.050 | 0.029 | 0.03 | 1.025 | 0.021 | 1.026 | 1.077 | 0.062 | 1.059 |
| $\psi$ = -1 | S235 | 54 | 1.25 | 0.055 | 0.029 | 0.03 | 1.033 | 0.025 | 1.000 | 1.006 | 0.006 | 1.007 |
| | S355 | 54 | 1.20 | 0.050 | 0.029 | 0.03 | 1.043 | 0.030 | 1.003 | 1.014 | 0.009 | 1.022 |
| | S420 | 54 | 1.20 | 0.050 | 0.029 | 0.03 | 1.045 | 0.034 | 1.008 | 1.015 | 0.011 | 1.023 |
| UDL | S235 | 54 | 1.25 | 0.055 | 0.029 | 0.03 | 1.016 | 0.012 | 1.008 | 1.018 | 0.013 | 1.007 |
| | S355 | 54 | 1.20 | 0.050 | 0.029 | 0.03 | 1.031 | 0.018 | 1.020 | 1.033 | 0.019 | 1.019 |
| | S420 | 54 | 1.20 | 0.050 | 0.029 | 0.03 | 1.037 | 0.020 | 1.017 | 1.039 | 0.021 | 1.017 |
| Point load | S235 | 54 | 1.25 | 0.055 | 0.029 | 0.03 | 1.021 | 0.013 | 1.001 | 1.016 | 0.011 | 1.004 |
| | S355 | 54 | 1.20 | 0.050 | 0.029 | 0.03 | 1.034 | 0.020 | 1.017 | 1.029 | 0.017 | 1.019 |
| | S420 | 54 | 1.20 | 0.050 | 0.029 | 0.03 | 1.038 | 0.022 | 1.016 | 1.033 | 0.020 | 1.017 |

**Table 9** Summary of the reliability analysis results for the proposed approach applied to stainless steel members subjected to different loading conditions assessed against benchmark FE results

| Load case | Grade | No. | $f_{y,mean}/f_{y,nom}$ | $V_{fy}$ | $V_{Wpl,y}$ | $V_E$ | Mode imperfection $e_{0,mod}$ | | | Lateral imperfection $e_{0,bow}$ | | |
|---|---|---|---|---|---|---|---|---|---|---|---|---|
| | | | | | | | $b$ | $V_\delta$ | $\gamma_{M1}^*$ | $b$ | $V_\delta$ | $\gamma_{M1}^*$ |
| $\psi$ = 1 | A | 54 | 1.20 | 0.050 | 0.029 | 0.03 | 1.046 | 0.020 | 1.004 | 1.057 | 0.029 | 1.008 |
| | D | 54 | 1.10 | 0.030 | 0.029 | 0.03 | 1.051 | 0.022 | 1.040 | 1.060 | 0.027 | 1.042 |
| | F | 54 | 1.15 | 0.055 | 0.029 | 0.03 | 1.056 | 0.030 | 1.047 | 1.068 | 0.039 | 1.055 |
| $\psi$ = 0.5 | A | 54 | 1.20 | 0.050 | 0.029 | 0.03 | 1.042 | 0.020 | 1.011 | 1.101 | 0.053 | 1.024 |
| | D | 54 | 1.10 | 0.030 | 0.029 | 0.03 | 1.049 | 0.026 | 1.051 | 1.106 | 0.052 | 1.061 |
| | F | 54 | 1.15 | 0.055 | 0.029 | 0.03 | 1.055 | 0.033 | 1.056 | 1.118 | 0.067 | 1.080 |
| $\psi$ = 0 | A | 54 | 1.20 | 0.050 | 0.029 | 0.03 | 1.040 | 0.021 | 1.014 | 1.125 | 0.077 | 1.069 |
| | D | 54 | 1.10 | 0.030 | 0.029 | 0.03 | 1.047 | 0.028 | 1.056 | 1.134 | 0.079 | 1.118 |
| | F | 54 | 1.15 | 0.055 | 0.029 | 0.03 | 1.051 | 0.034 | 1.061 | 1.141 | 0.090 | 1.133 |
| $\psi$ = -0.5 | A | 54 | 1.20 | 0.050 | 0.029 | 0.03 | 1.047 | 0.028 | 1.016 | 1.123 | 0.083 | 1.090 |
| | D | 54 | 1.10 | 0.030 | 0.029 | 0.03 | 1.053 | 0.033 | 1.061 | 1.134 | 0.088 | 1.150 |
| | F | 54 | 1.15 | 0.055 | 0.029 | 0.03 | 1.056 | 0.038 | 1.064 | 1.137 | 0.095 | 1.151 |
| $\psi$ = -1 | A | 54 | 1.20 | 0.050 | 0.029 | 0.03 | 1.111 | 0.077 | 1.081 | 1.063 | 0.044 | 1.033 |
| | D | 54 | 1.10 | 0.030 | 0.029 | 0.03 | 1.117 | 0.076 | 1.124 | 1.066 | 0.044 | 1.074 |
| | F | 54 | 1.15 | 0.055 | 0.029 | 0.03 | 1.117 | 0.082 | 1.128 | 1.067 | 0.048 | 1.077 |
| UDL | A | 54 | 1.20 | 0.050 | 0.029 | 0.03 | 1.051 | 0.023 | 1.004 | 1.055 | 0.027 | 1.007 |
| | D | 54 | 1.10 | 0.030 | 0.029 | 0.03 | 1.057 | 0.026 | 1.041 | 1.061 | 0.028 | 1.043 |
| | F | 54 | 1.15 | 0.055 | 0.029 | 0.03 | 1.062 | 0.035 | 1.052 | 1.066 | 0.038 | 1.056 |
| Point load | A | 54 | 1.20 | 0.050 | 0.029 | 0.03 | 1.055 | 0.026 | 1.005 | 1.051 | 0.024 | 1.006 |
| | D | 54 | 1.10 | 0.030 | 0.029 | 0.03 | 1.063 | 0.029 | 1.042 | 1.060 | 0.027 | 1.043 |
| | F | 54 | 1.15 | 0.055 | 0.029 | 0.03 | 1.067 | 0.038 | 1.053 | 1.063 | 0.036 | 1.053 |

**Table 10** Summary of comparisons between ultimate member resistances obtained from different design methods for worked examples

| Imperfection $e_0$ | Analysis | Cross-section check | Example 1 | | Example 2 | |
|---|---|---|---|---|---|---|
| | | | $M_u/M_{pl,y}$ | $M_u/M_{FE}$ | $M_u/M_{pl,y}$ | $M_u/M_{FE}$ |
| Benchmark $L$/1000 + R.S. | GMNIA | CSM strain limit | 0.671 | - | 0.674 | - |
| $e_{0,mod}$ | GMNIA | CSM strain limit | 0.663 | 0.988 | 0.668 | 0.991 |
| $e_{0,bow}$ | GMNIA | CSM strain limit | 0.653 | 0.973 | 0.669 | 0.993 |
| $e_{0,LT,pl,b\text{-}c}$ | GNIA | Linear plastic check | 0.705 | 1.051 | 0.619 | 0.918 |
| $e_{0,LT,pl,tab}$ | GNIA | Linear plastic check | 0.610 | 0.909 | 0.551 | 0.818 |
| Member buckling check $M_{EC3}$ | - | - | 0.569 | 0.848 | 0.503 | 0.746 |